

## Process optimization of Auramine O adsorption by surfactant-modified activated carbon using Box–Behnken design of response surface methodology

Rahmat Ali, Tahira Mahmood\*, Abdul Naeem, Abid Ullah,  
Madeeha Aslam, Sheraz Khan

National Center of Excellence in Physical Chemistry, University of Peshawar, Peshawar 25120, Pakistan,  
Tel. +92 919216766; email: tahiramahmood@uop.edu.pk (T. Mahmood)

Received 8 April 2020; Accepted 17 October 2020

### ABSTRACT

The present study explores the sorption capacity of anionic surfactant, sodium dodecylsulfate (SDS)-modified activated carbon (PA-AC-SDS) for highly toxic and carcinogenic dye, Auramine O (AO) from aqueous systems. The effects of various process variables such as dye solution pH, adsorbent dose, dye initial concentration and contact time have been explored via Box–Behnken design of response surface methodology. Optimum conditions were found to be solution pH of 6.00, adsorbent dose of 0.110 g, contact time of 240 min and dye initial concentration of 1,000 mg L<sup>-1</sup>, under which the measured experimental adsorption capacity for AO was 425.060 mg g<sup>-1</sup>, which was in close agreement with the predicted value (427.130 mg g<sup>-1</sup>), with relative error of -0.490%. Adsorption kinetics and isotherm data were well described by pseudo-second-order kinetics and Langmuir isotherm model. Intra-particle diffusion and Boyd's models showed that both film diffusion and intra-particle diffusion may occur parallel during the interaction of the AO with PA-AC-SDS. Thermodynamic investigations presented spontaneous and endothermic nature of adsorption. In addition, regeneration studies revealed that PA-AC-SDS was effective in removal of AO for five consecutive cycles, showing it to be an efficient technology for textile industries effluents.

*Keywords:* Adsorption; Auramine O; Activated carbon; Sodium dodecylsulfate; Box–Behnken design; Optimization; Modeling

### 1. Introduction

Water is an essential constituent of human life and ecosystem on the earth. It is a major resource of food, health, clothing and environment. The demand of water has increased with the rise in world's population. But the augmented industrial activities and advancement in living standards, exploited the natural water resource. Nowadays, a large number of industries release a variety of hazardous compounds such as heavy metals, drugs, pesticides, and dyes to ocean, lakes and rivers [1–4]. Among these pollutants, dyes are the organic noxious waste that are produced by textile, plastics, rubber, printing, electroplating, and paper making industries. Almost all dyes are extremely

poisonous, mutagenic, non-biodegradable and carcinogenic due to its complex aromatic structure. The annual production of commercial dyes across the world is  $7 \times 10^5$  tons, while, 5%–10% of these dyes are discharged from industries to aqueous environment without any treatment [3,5,6]. AO is a cationic dye applied in coloring leather, food, carpet, paper and textiles. Beside the commercial importance, the presence of AO in water even in trace amount is highly injurious and has been proved as carcinogenic by International Agency for Research on Cancer [7]. Considering the highly toxic and carcinogenic nature of AO, its removal from aqueous systems is highly desired before their discharge into natural environment to save human life and the ecosystem.

\* Corresponding author.

A number of techniques such as membrane filtration, reverse osmosis, flocculation, radiolysis, advanced oxidation, ozonation, aerobic–anaerobic, electrochemical treatment and adsorption are employed for the treatment of dye-containing effluents [1,8–10]. Most of these techniques are expensive and less efficient that might limit its applicability in underdeveloped countries. However, among these methods, adsorption is a more frequently used method because of its effectiveness, flexibility, simplicity and least cost [1,5]. A wide range of available adsorbents (lignocellulose, silica, coal, clay, zeolite, chitin, nano-adsorbents, biomass, etc.) have been tested by researchers for treatment of dye-contaminated wastewater [1,3,8,11–13]. But activated carbon (AC) is the most favorable and effective adsorbent for environmental application. It has been utilized extensively for the uptake of dyes and many other organic and inorganic hazardous substances from aqueous systems owing to its large surface area and variety of active groups.

The surface chemical properties of AC can be modified by various physical and chemical methods such as thermal or steam treatment, using acids or bases and through impregnation of foreign materials to exhibit improved pollutant removal [14]. Surface modification with anionic surfactants has improved AC efficiency for cationic dyes and heavy metals adsorption from wastewater [12,15]. Anionic surfactant, sodium dodecylsulfate (SDS), contains many oxygen-based functional groups that get adsorbed at the surface of AC and enhances its properties at the interface. The presence of SDS increases dye removal efficiency of AC as well as encourages selective adsorption [8,12,15–17]. Nadeem et al. [15] used SDS-modified carbon adsorbent for Cd(II) removal with good adsorption efficiency (95.6%). Ahn et al. [12] and Song et al. [18] efficiently utilized SDS-impregnated AC for removal Cd(II) and Pb(II), respectively. Likewise, Moradi [19] prepared SDS-functionalized ordered mesoporous carbon through microwave heating and studied its feasibility for methylene blue uptake and the adsorption efficiency was found to be 88.4%.

In the current study, it was attempted to modify the surface of waste tea-based AC with anionic surfactant SDS and to explore its efficiency for removal of basic dye AO from aqueous systems. The influence of different variables on adsorption process was studied and optimized successfully using response surface methodology (RSM)–based Box–Behnken design. RSM is a technique for optimization of conditions in which the best possible response can be determined. RSM method is efficiently utilized to assess individual and interactive effects of process parameters on the response of dye removal and optimize the response efficiency [20].

In the literature, many studies had reported the removal of AO from aqueous media using AC synthesized from a variety of agricultural-based materials. However, no study described the use of SDS-modified AC for AO removal from aqueous systems. As far as our knowledge is concerned, this is the first article manipulating the potential of SDS-modified AC for effective removal of highly toxic carcinogenic dye, AO, from aqueous systems by considering the effect of different process parameters. Box–Behnken design of RSM was selected to investigate the effects of major process variables based on dye adsorption capacity as

response. Furthermore, the adsorption mechanism, kinetics, isotherm and thermodynamic aspects were also studied.

## 2. Experimental setup

### 2.1. Materials and chemicals

The chemicals used in the present study were of analytical grade and highest purity. Sodium hydroxide (99.99%), hydrochloric acid (37%), sodium chloride (99%), sodium carbonate (99.5%), sodium hydrogen carbonate (99.10%) were purchased from Scharlau, Spain. SDS ( $\text{CH}_3(\text{CH}_2)_{11}\text{OSO}_3\text{Na}$ ) was supplied by KOSDAQ Chemicals Co. Ltd., (South Korea). Cationic dye, AO (80%), was purchased from Sigma-Aldrich, Germany. The chemical structure and various other properties of AO are presented in Table 1. The operational standard solutions of desired strength were prepared in double distilled water. Stock solution of AO ( $1,000 \text{ mg L}^{-1}$ ) was prepared and was subsequently diluted to acquire the solutions of desired strength for conducting experiments.

### 2.2. Preparation of AC

AC with surface area of  $1,136.240 \text{ m}^2 \text{ g}^{-1}$  and pore volume of  $0.860 \text{ cm}^3 \text{ g}^{-1}$  was prepared from used tea leaves via impregnation with  $\text{H}_3\text{PO}_4$  under optimal operational parameters as reported in our previous work [21]. This AC served as starting material to prepare the surfactant-modified AC.

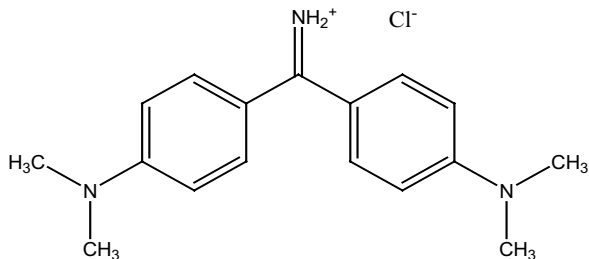
### 2.3. Modification of AC with SDS

The surface of AC prepared via chemical activation with phosphoric acid was modified with anionic surfactant, SDS to enhance its efficiency for removal of basic dyes from aqueous solutions. Modification of AC surface with SDS was carried out as follows: a definite amount of AC (2.5 g) was taken in a 1-L round bottom flask and 125 mL aqueous solution of SDS ( $30 \text{ mmol L}^{-1}$ ) was added to it. The contents of the flask were shaken at  $70^\circ\text{C}$  for 24 h at 120 rpm using thermostatic shaker bath. After that the mixture was kept undisturbed for 30 min and the AC particles were separated by passing the mixture through a filtering medium. The product obtained was washed with double distilled water and oven dried at  $60^\circ\text{C}$  until all the moisture was removed. The material obtained after treatment with SDS was labeled as PA-AC-SDS and was kept in quick fit vessels for further studies.

### 2.4. Surface and chemical characterization

The surface area and porous texture of PA-AC-SDS were assessed by  $\text{N}_2$  adsorption–desorption isotherms at 77 K, via a surface area and pore size analyzer (ASAP-2010M+C, Micromeritics Instrument Corp., USA). The carbon sample was outgassed at 423 K for 4 h in inert environment of  $\text{N}_2$  before initiating the isotherm. Surface area of the sample was evaluated from the quantity of  $\text{N}_2$  adsorbed at  $P/P_0$  value of 0.95 using Brunauer, Emmett and Teller (BET) equation, while pore-size distributions were estimated by the Barrett–Joyner–Halenda method [21,22]. Surface morphology and porous structure were observed via scanning

Table 1  
Properties and structure of AO

Commercial name	Auramine O
Abbreviation	AO
Color index (C.I.) name	Basic Yellow 2
IUPAC name	4-[4-(Dimethylamino) benzenecarboximidoyl]-N,N-dimethylaniline; hydrochloride
C.I. No.	41000
Molecular formula	$C_{17}H_{22}ClN_3$
Class	Diarylmethane
Molar mass ( $g\ mol^{-1}$ )	303.830
Water solubility	10 mg/mL
Chemical class	Cationic
Ionization	Basic
$\lambda_{max}$ (nm)	432
Structure	

electron microscope (SEM, JEOL-JSM-5910, Japan). To obtain an insight on the elemental composition of adsorbent, energy dispersive X-ray (EDX) and CHNS analysis were carried out using EDX micro analyzer spectrometer (INCA-200, UK) and CHNS analyzer (LECO CHNS-932, St. Joseph, USA). X-rays diffraction (XRD) examination of the modified sample was carried out by JEOL X-ray diffractometer (model JDX-3532). Boehm's titration and Fourier-transform infrared spectroscopic (FTIR) analysis were applied to evaluate different functional groups on PA-AC-SDS surface in the scanning range of  $4,000\text{--}400\text{ cm}^{-1}$  using PerkinElmer FTIR-2000 (United States). Zero point charge ( $pH_{PZC}$ ) was assessed by applying solid addition method [23]. Furthermore, proximate analysis was conducted using American Standard Testing Methods for materials, ASTM D1762-84.

### 2.5. Adsorption protocol

The capacity of PA-AC-SDS for AO removal was evaluated by batch method. The adsorption tests were performed in an array of 100 mL polythene bottles by contacting a definite volume (40 mL) of dye solution of desired concentration and a fixed quantity of adsorbent. The dye aqueous solutions were agitated in end-to-end shaker bath (SHEL LAB, WS 17-2, USA) at constant temperature shaking speed of 120 rpm to ensure equilibrium. A 0.10 M solution of HCl or/and NaOH was used for pH adjustment using a pH meter (NeoMet, pH 250 L, Korea). All the adsorption tests were performed in triplicate and the average value was utilized in data manipulation. The influence of various process variables such as pH of dye solution, media dosage, shaking time and dye initial concentration on AO

uptake was studied in 29 experiments, designed by three levels Box–Behnken with details given in Tables 2 and 3. At the end of each experiment, the dye solutions were centrifuged to isolate the adsorbent particles. The remaining concentration of dye in solution was evaluated spectrophotometrically at the corresponding wavelength ( $\lambda_{max}$  432 nm). The dye adsorption capacity,  $q_e$  ( $mg\ g^{-1}$ ), was evaluated as follows:

$$q_e = \frac{V(C_0 - C_e)}{w} \quad (1)$$

where  $C_0$  and  $C_e$  are the liquid-phase dye initial and equilibrium concentrations ( $mg\ L^{-1}$ ), respectively,  $V$  is the volume (L) and  $w$  is the adsorbent weight (g).

### 2.6. Effect of process variables on AO adsorption

#### 2.6.1. Experimental design

The various operation parameters affecting AO adsorption capacity by PA-AC-SDS were optimized based on standard RSM design known as Box–Behnken design (BBD). Four factors and three levels BBD method was carefully chosen as experimental design as it can reduce excessive tests and hence the overall reaction cost. It also helps to explore the individual and combined effects of the various process parameters and to find the best operational parameters [24]. The independent variables to be optimized were pH of dye solution ( $X_1$ ), PA-AC-SDS dosage ( $X_2$ ), shaking time ( $X_3$ ) and dye initial concentration ( $X_4$ ). These parameters and their corresponding ranges have been

chosen on the basis of previous investigations and pilot study carried out before manipulating this experiment. The input variables and levels with their corresponding values are given in Table 2. The uptake capacity of AO was

taken as response variable ( $Y$ ), which is correlated to the independent variables using a second-order polynomial equation [25] as:

$$Y = b_0 + \sum_{i=1}^k b_i X_i + \sum_{i=1}^k b_{ii} X_i^2 + \sum_{i=1}^{k-1} \sum_{j=1}^k b_{ij} X_i X_j + e \tag{2}$$

Table 2  
Independent variables and their coded levels of Box–Behnken design for AO uptake by PA-AC-SDS

Variables	Code	Units	Coded Variable Levels		
			-1	0	+1
pH	$X_1$	–	2.000	6.000	10
Adsorbent dose	$X_2$	g	0.010	0.110	0.200
Contact time	$X_3$	min	10	125	240
AO concentration	$X_4$	mg L <sup>-1</sup>	100	550	1,000

where  $Y$  is the predicted response,  $k$  is number of input variables,  $b_0$  is the model constant,  $b_i$ ,  $b_{ii}$  and  $b_{ij}$  are the measures of the linear ( $X_i$ ), quadratic ( $X_i^2$  and  $X_j^2$ ) and interaction ( $X_i X_j$ ) effects, respectively while,  $e$  is the residual error. Each input variable consists of three levels, which represents lower (-1), higher (+1) and central points (0) for the optimum removal of AO. The total number of experimental runs ( $N$ ) in this design can be evaluated using Eq. (3) as:

Table 3  
Experimental design matrix for AO adsorption onto PA-AC-SDS and comparison of actual and predicted response results using Box–Behnken design of RSM

Run	Variables						Response ( $Y$ )			
	Solution pH $X_1$		Adsorbent dosage (g) $X_2$		Time (min) $X_3$		AO initial concentration (mg L <sup>-1</sup> ) $X_4$		AO adsorption capacity, $q_e$ (mg g <sup>-1</sup> )	
	Coded	Actual	Coded	Actual	Coded	Actual	Coded	Actual	Experimental	Predicted
1	0	6.000	0	0.110	-1	10.000	-1	100.000	60.010	63.580
2	0	6.000	1	0.200	0	125.000	-1	100.000	61.130	55.660
3	0	6.000	0	0.110	-1	10.000	1	1,000.000	280.720	283.320
4	0	6.000	-1	0.010	0	125.000	-1	100.000	88.570	97.260
5	1	10.000	0	0.110	0	125.000	1	1,000.000	345.890	340.760
6	0	6.000	1	0.200	1	240.000	0	550.000	235.250	231.040
7	1	10.000	0	0.110	0	125.000	-1	100.000	19.670	14.690
8	0	6.000	1	0.200	0	125.000	1	1,000.000	320.610	316.260
9	0	6.000	0	0.110	0	125.000	0	550.000	281.480	281.690
10	1	10.000	1	0.200	0	125.000	0	550.000	157.790	169.850
11	0	6.000	0	0.110	1	240.000	-1	100.000	52.420	54.190
12	-1	2.000	0	0.110	1	240.000	0	550.000	175.340	181.730
13	0	6.000	-1	0.010	1	240.000	0	550.000	320.420	314.850
14	0	6.000	0	0.110	0	125.000	0	550.000	281.660	281.690
15	0	6.000	-1	0.010	-1	10.000	0	550.000	245.660	241.160
16	0	6.000	1	0.200	-1	10.000	0	550.000	173.430	170.300
17	-1	2.000	0	0.110	0	125.000	1	1,000.000	280.670	276.930
18	1	10.000	0	0.110	1	240.000	0	550.000	235.460	236.260
19	-1	2.000	-1	0.010	0	125.000	0	550.000	220.770	213.080
20	0	6.000	0	0.110	0	125.000	0	550.000	281.440	281.690
21	-1	2.000	1	0.200	0	125.000	0	550.000	133.660	138.750
22	-1	2.000	0	0.110	-1	10.000	0	550.000	131.420	134.950
23	0	6.000	0	0.110	1	240.000	1	1,000.000	426.320	427.130
24	1	10.000	0	0.110	-1	10.000	0	550.000	150.660	148.610
25	0	6.000	0	0.110	0	125.000	0	550.000	281.910	281.690
26	-1	2.000	0	0.110	0	125.000	-1	100.000	13.910	10.330
27	0	6.000	-1	0.010	0	125.000	1	1,000.000	419.530	429.330
28	0	6.000	0	0.110	0	125.000	0	550.000	281.950	281.690
29	1	10.000	-1	0.010	0	125.000	0	550.000	250.890	250.180

$$N = 2k(k-1) + C_0 \tag{3}$$

where  $k$  is the number of independent variables and  $C_0$  is the number of central points. A total of 29 runs were carried out in the present study, which consists of 24 trial and 5 central points. The center points were used to calculate the experimental error.

### 2.6.2. Model fitting

The adsorption of AO by PA-AC-SDS was studied in the ranges of independent variables. Design-Expert software (version 7.0.0, Stat-Ease, Inc., Minneapolis, USA) [26] was employed for statistical analysis, evaluating model suitability and 3D response surface plots. Contour and response surface plots were used to observe the relationship between the input parameters and response. The statistical significance of variables and fit between the model and experimental data was assessed using analysis of variance (ANOVA). The coefficient of determination ( $R^2$ ),  $F$ -values (Fisher variation ratio), probability  $p$ -value, and adequate precision (AP) were used to determine the adequacy and fitting quality of the selected model and significance of input variables [27].

### 2.7. Adsorption kinetics and mechanism

The kinetics of AO adsorption was investigated at various time intervals ranging from 10 to 240 min. Adsorbent mass of 100 mg was taken in 100 mL polythene bottles containing 40 mL of dye solution (100, 200, 300 and 400 mg L<sup>-1</sup>) and the mixture was agitated at 120 rpm at 298 ± 1 K until the point of saturation was achieved. The amount of AO adsorbed at time  $t$ ,  $q_t$  (mg g<sup>-1</sup>), was measured using the mass-balance relation:

$$q_t = \frac{V(C_0 - C_t)}{m} \tag{4}$$

where  $C_t$  is the liquid-phase dye concentrations (mg L<sup>-1</sup>) at a given interval  $t$  (min). To investigate the kinetics and mechanism of AO uptake by PA-AC-SDS, pseudo-first-order [28], pseudo-second-order [29,30], Elovich [31] and intra-particle diffusion [32] models were used to fit the experimental data. The pseudo-first-order model in its linear form is given as follows:

$$\log(q_e - q_t) = \log q_e - \left(\frac{k_1}{2.303}\right)t \tag{5}$$

where  $k_1$  (min<sup>-1</sup>) is the pseudo-first-order rate constant while  $q_e$  and  $q_t$  are the uptake capacities (mg g<sup>-1</sup>) of PA-AC-SDS at the point of saturation and at interval  $t$ , respectively.

Pseudo-second-order kinetic model equation in linearized form, given by Ho's can be represented as follows:

$$\frac{t}{q_t} = \frac{1}{k_2 q_e^2} + \frac{1}{q_e} t \tag{6}$$

where  $k_2$  is the pseudo-second-order rate constants (g mg<sup>-1</sup> min<sup>-1</sup>). The initial adsorption rate,  $h$  (mg g<sup>-1</sup> min<sup>-1</sup>), at  $t \rightarrow 0$  is given,  $h = k_2 q_e^2$ .

The Elovich model equation applied to kinetic data is expressed as follows:

$$q_t = \frac{1}{\beta} \ln(\alpha\beta) + \frac{1}{\beta} \ln t \tag{7}$$

where  $\alpha$  is the initial adsorption rate (mg g<sup>-1</sup> min<sup>-1</sup>) and  $\beta$  (g mg<sup>-1</sup>) is related to the magnitude of surface coverage and energy of activation.

Intra-particle diffusion model was applied to verify the influence of mass-transfer resistance offered to the adsorption of dye molecules by PA-AC-SDS and to observe the probability of pore diffusion as the rate-limiting step. The linear form of intra-particle diffusion model can be represented by the equations as follows:

$$q_t = k_i t^{1/2} + C \tag{8}$$

where  $k_i$  (mg g<sup>-1</sup> min<sup>-1/2</sup>) is the rate constant at a given stage  $i$  for intra-particle diffusion model while  $C$  (mg g<sup>-1</sup>) is associated to the thickness of boundary layer. The Boyd's model [33] was applied to further confirm the rate-limiting step and mechanism involved in the uptake of AO by PA-AC-SDS. The different parameters were calculated using the equations as given follows:

$$F = 1 - \frac{6}{\pi^2} \exp(-B_i) \tag{9}$$

where  $F$  is the fractional uptake of AO at a given interval  $t$  that could be determined as  $F = q_t/q_e$  while  $B_i$  is a mathematical function of  $F$ , which can be estimated from the equation given as follows:

$$B_i = -0.4977 - \ln(1 - F) \tag{10}$$

### 2.8. Adsorption equilibrium

Equilibrium isotherm studies were executed by changing AO initial concentration from 100 to 1,000 mg L<sup>-1</sup> at constant PA-AC-SDS weight. Dye solutions pH was kept at optimal value (6.00) and shaken for 240 min at constant temperature (293, 303, 313 and 323 K) using thermostatic shaker bath. The dye amount removed at the point of saturation was determined using Eq. (1). To explain the behavior of AO uptake by PA-AC-SDS, equilibrium data were analyzed using four hypothetical models as, Langmuir [34], Freundlich [35], Temkin [36] and Dubinin-Radushkevich (D-R) [37] isotherm equations.

Langmuir model suggests monolayer formation of adsorbate molecules on a homogeneous adsorbent surface with same adsorption energies. The Langmuir isotherm model in its linear form can be expressed as follows:

$$\frac{C_e}{q_e} = \frac{1}{K_L q_m} + \frac{C_e}{q_m} \tag{11}$$

where  $q_m$  ( $\text{mg g}^{-1}$ ) is a single-layer uptake capacity and the Langmuir constant  $K_L$  ( $\text{L mg}^{-1}$ ) is associated to the adsorption energy. The important features of Langmuir model can be represented by a dimensionless equilibrium element, termed as separation factor ( $R_L$ ), that gives evidence about the favorability of adsorption process and can be defined [38] as:

$$R_L = \frac{1}{1 + K_L C_0} \quad (12)$$

where  $C_0$  is the dye initial concentration ( $\text{mg L}^{-1}$ ),  $K_L$  is the Langmuir constant that corresponds to the energy of sorption sites ( $\text{L mg}^{-1}$ ). The value of  $R_L$  can be used to evaluate the favorability of Langmuir isotherm.  $R_L$  value lies between 0 and 1 (favorable),  $R_L$  value greater than 1 (unfavorable),  $R_L$  equal to zero (irreversible), or  $R_L$  equal to one (linear) [39].

Freundlich isotherm model assumes multi-layer adsorption on heterogeneous adsorbent surfaces with adsorption sites of different energies. The linear form of Freundlich model can be depicted as follows:

$$\ln q_e = \ln K_F + \frac{1}{n} \ln C_e \quad (13)$$

where  $K_F$  ( $\text{mg g}^{-1} (\text{L mg}^{-1})^{1/n}$ ) is Freundlich isotherm constant related to uptake capacity while  $1/n$  is heterogeneity parameter that corresponds to adsorption intensity, which reflects favorability of sorption process.

Temkin isotherm model gives clue related to adsorbate-adsorbent interaction and suggests that for all adsorbate molecules heat of adsorption falls linearly with surface coverage as a result of adsorbate-adsorbent interactions. Temkin isotherm model linear form can be expressed as follows:

$$q_e = \frac{RT}{b_T} \ln K_T + \frac{RT}{b_T} \ln C_e \quad (14)$$

where  $K_T$  ( $\text{L g}^{-1}$ ) is the steadiness constant corresponding to the highest binding energy,  $b_T$  ( $\text{J mol}^{-1}$ ) is related to heat of adsorption,  $R$  ( $8.314 \text{ J mol}^{-1} \text{ K}^{-1}$ ) is universal gas constant and  $T$  ( $\text{K}$ ) is absolute temperature.

Dubinin-Radushkevich (D-R) model was applied to distinguish whether the sorption route is physical, chemical or ion exchange. The D-R model is expressed as follows:

$$\ln q_e = \ln q_{D-R} - \beta \varepsilon^2 \quad (15)$$

where constant  $q_{D-R}$  is theoretical isotherm adsorption capacity ( $\text{mg g}^{-1}$ ),  $\varepsilon$  is the Polanyi potential equivalent to  $RT \ln(1 + 1/C_e)$  and the constant  $\beta$  ( $\text{mol}^2 \text{ J}^{-2}$ ) is associated to the mean adsorption energy  $E$  ( $\text{kJ mol}^{-1}$ ) through the following equation:

$$E = \frac{1}{\sqrt{2\beta}} \quad (16)$$

The value of  $E$  can be used to determine the type of mechanism involved in the uptake process. In case,  $E$  value lower than  $8 \text{ kJ mol}^{-1}$  indicates physisorption,

lies between 8 and  $16 \text{ kJ mol}^{-1}$  implies ion exchange mechanism, or the range of 20 to  $40 \text{ kJ mol}^{-1}$  indicating chemisorption [40].

### 2.9. Adsorption thermodynamics

Thermodynamic parameters for AO removal were studied to evaluate the adsorption characteristic and to find the nature of uptake process. The various thermodynamic parameters such as Gibbs free energy ( $\Delta G^\circ$ ), enthalpy ( $\Delta H^\circ$ ) and entropy ( $\Delta S^\circ$ ) were determined at different temperatures using the following equations [41].

$$\ln K_L = -\frac{\Delta H^\circ}{RT} + \frac{\Delta S^\circ}{R} \quad (17)$$

$$\Delta G^\circ = \Delta H^\circ - T\Delta S^\circ \quad (18)$$

where  $R$  ( $8.314 \text{ J mol}^{-1} \text{ K}^{-1}$ ) is the general gas constant while  $T$  ( $\text{K}$ ) is the solution temperature and  $K_L$  ( $\text{L mg}^{-1}$ ) is Langmuir constant. The values of  $\Delta S^\circ$  and  $\Delta H^\circ$  were correspondingly calculated from the intercept and slope of  $\ln K_L$  vs.  $1/T$  plot.

### 2.10. Desorption experiments

For desorption study, a known quantity of dye-loaded surface (PA-AC-SDS) was immersed in 40 mL of different desorbing medium and shaken at 120 rpm for 240 min. At the end of desorption experiments, adsorbent was separated from desorption medium and AO concentrations were measured spectrophotometrically. The amount of dye released from adsorbent surface was measured and the surface collected was rinsed, dried and recycled. Five successive adsorption-desorption cycles were carried out. The percentage of dye desorbed was determined using the equation as given below [42]:

$$\% \text{ Desorption} = \frac{C_d}{C_0 - C_e} \times 100 \quad (19)$$

where  $C_0$  and  $C_e$  are AO concentrations ( $\text{mg L}^{-1}$ ) in solution, initially taken and after the point of equilibration while  $C_d$  ( $\text{mg L}^{-1}$ ) is the concentration at the end of desorption test.

## 3. Results and discussion

### 3.1. Adsorbent characterization

#### 3.1.1. Surface morphology

The SEM images of PA-AC-SDS (before and after dye uptake) are presented in Figs. 1a and b, respectively. The external surface of PA-AC-SDS (Fig. 1a) seems as rough and porous with numerous pores of non-uniform size, shape, distribution and appeared to be coated due to the distribution of surfactant molecules on its entire surface. SDS modification caused a slight reduction in  $S_{\text{BET}}$  accompanied by reduction in pore volumes of PA-AC-SDS relative to its precursor non-modified AC. The SEM micrographs also revealed that there is no observable particles aggregation,

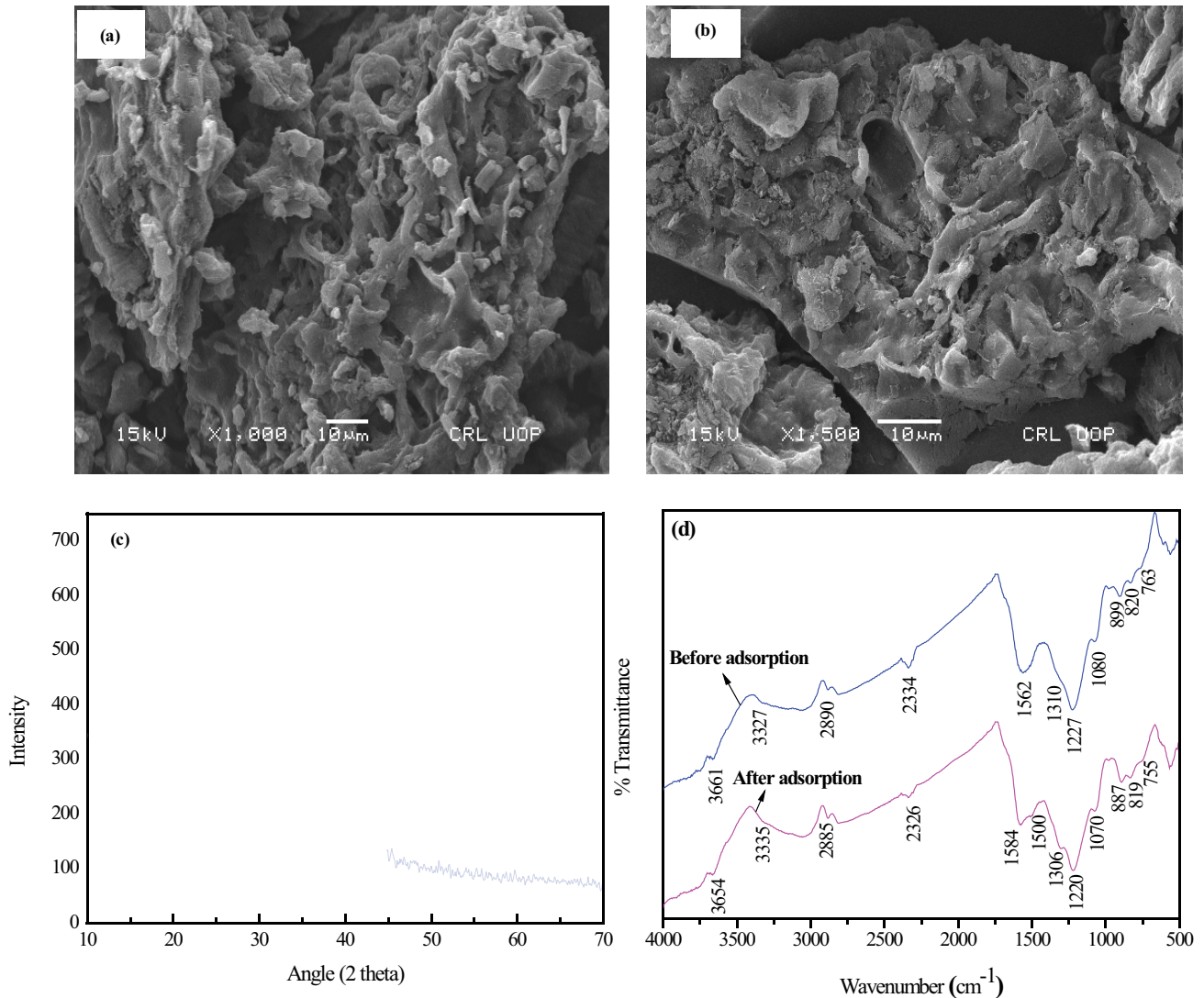


Fig. 1. Scanning electron micrographs (a) before and (b) after adsorption, (c) X-rays diffraction pattern and (d) FTIR spectra of PA-AC-SDS.

which shows that most of the SDS molecules are adhered to adsorbent surface by their non-polar tails with their polar heads oriented outside, which may be responsible for negative surface properties of the adsorbent [43]. After AO uptake, SEM micrographs of the sample (Fig. 1b) show a visible change in surface morphology with majority of the pores vanished. This may be attributable to the saturation and pore filling by the dye molecules.

### 3.1.2. BET surface area and XRD analysis

Table 6 shows the BET surface area ( $S_{\text{BET}}$ ) and pore size distribution of the adsorbent estimated from  $\text{N}_2$  adsorption isotherms. Even though the surfactant-modified sample (PA-AC-SDS) has well-developed porous structure, good surface area and considerable number of mesopores and micropores, it was observed that modification with SDS is accompanied by a small reduction in the sample surface area and pore volume. Before modification, the BET surface

area and micropore volume of precursor AC were found to be  $1,136.240 \text{ m}^2 \text{ g}^{-1}$  and  $0.470 \text{ cm}^3 \text{ g}^{-1}$ , respectively. However, after modification with anionic surfactant SDS, the  $S_{\text{BET}}$  and micropore volume of PA-AC-SDS were correspondingly decreased to  $1,114.390 \text{ m}^2 \text{ g}^{-1}$  and  $0.440 \text{ cm}^3 \text{ g}^{-1}$  that could be associated to overcrowding and blocking of pores by the hydrophobic paraffinic tails of SDS molecule [16].

XRD examination of PA-AC-SDS was accomplished and the resultant spectrum is given in Fig. 1c. As can be observed in the XRD pattern, the weak broad peak at  $2\theta$  value of about  $25^\circ$  is assigned to the amorphous carbon [44]. Amorphous nature is an important characteristic of highly porous materials such as ACs having high adsorption efficiencies for both organic and inorganic contaminants.

### 3.1.3. FTIR analysis

In order to examine surface chemistry of SDS-modified activated carbon (PA-AC-SDS) before and after

dye uptake, FTIR study was performed and the resultant spectra are presented in Fig. 1d. The band in the region of  $3,661\text{ cm}^{-1}$  was attributed to O–H stretching vibrations of intra and inter-molecular hydrogen bonding of carboxylic, phenolic and alcoholic groups [45]. The weak band at about  $3,327\text{ cm}^{-1}$  was attributed to O–H and N–H stretching vibration of carboxyl and amine functionality [46]. The band in the region of  $1,500\text{--}1,562\text{ cm}^{-1}$  was assigned to aromatic ring bond vibrations and C–O axial bending of carboxylic, lactones and phenolic groups [47]. The absorption bands at  $1,227\text{ cm}^{-1}$  may be due to an asymmetric stretching of C–O–S and the band around  $1,080\text{ cm}^{-1}$  correspond to the symmetric stretching of S=O [48,49]. FTIR spectrum of PA-AC-SDS displays a representative band at  $2,890\text{ cm}^{-1}$  attributed to  $\text{CH}_2$  groups of SDS and also a feeble band at  $1,310\text{ cm}^{-1}$  related to stretching vibration of  $\text{SO}_3$  group. These investigations provide the evidence that AC has been successfully modified with SDS through hydrophobic interactions. The bands around  $899\text{--}834\text{ cm}^{-1}$  and  $763\text{ cm}^{-1}$  are ascribed to  $\text{OC-OH}$  group and C–H groups. After AO adsorption, the intensity of the peaks, located at  $3,661$ ;  $3,327$ ;  $2,890$ ;  $2,562$ ;  $1,227$ ;  $1,080$ ;  $899$  and  $820\text{ cm}^{-1}$  decreased and shifted to  $3,654$ ;  $3,335$ ;  $2,885$ ;  $1,584$ ;  $1,210$ ;  $1,070$ ;  $887$  and  $819\text{ cm}^{-1}$ , respectively, representing the contribution of these functional groups in dye uptake and presence of van der Waals interactions among AO molecules and the active sites on PA-AC-SDS surface.

#### 3.1.4. Boehm's titration analysis

The surface chemistry and adsorption property of AC samples depend on the types and amount of various active functionalities on their surfaces. The contents of these groups on PA-AC-SDS surface were evaluated using Boehm's titration technique and are listed in Table 6. It was found that PA-AC-SDS has considerable amount of acidic groups. However, after modification with SDS, the concentration of carboxylic and phenolic groups was correspondingly decreased from  $1.270$  to  $1.010\text{ mmol g}^{-1}$  and  $1.250$  to  $0.720\text{ mmol g}^{-1}$ . But the concentration of total basic functionalities augmented from  $0.130$  to  $0.290\text{ mmol g}^{-1}$  relative to its precursor AC. Similar results have been investigated by Wei et al. [50] for AC modified with sodium dodecyl benzene sulfonate using microwave heating. As the polar heads of SDS can act as basic functionality, thus boosts basicity of PA-AC-SDS suggesting that the adsorbent surface is covered by SDS molecules. Furthermore, the point of zero charge of the sample was raised to  $5.110$  from  $4.110$  of its precursor AC. This can be attributed to the decrease in content of carboxylic and phenolic functionalities and expansion in the amount of carbonyl functionalities, which have high  $\text{pK}_a$  value ( $\text{pK}_a \sim 16\text{--}20$ ) [12,51].

#### 3.1.5. Proximate and elemental analysis

The ASTM technique (ASTM-D1762-84) was used to evaluate the proximate and elemental analysis of PA-AC-SDS. Results (Table 6) show that PA-AC-SDS has high fixed carbon and little moisture and ash content, which is one of the criteria for a competent and good-quality adsorbent for treating dyes containing aqueous systems.

Elemental analysis revealed that compared with the precursor AC, oxygen percentage of PA-AC-SDS was raised from  $16.240\%$  to  $19.910\%$  after modification with SDS. The increase in oxygen content may be due to the rise in oxygen containing surface groups on PA-AC-SDS surface caused by oxygen-rich SDS molecules during modification. Figs. 2a and b display the EDX spectra and percentage of different elements of PA-AC-SDS before and after dye uptake, respectively. The key elements observed were C, O, P, S, Na and N, which have been derived from precursor AC and SDS. A minute quantity of Ca and Cu were also found that may be related to the nature and source of the starting material. It is also observable from Fig. 2a that PA-AC-SDS has considerable amount of sulfur and higher content of oxygen shown that the precursor AC has been successfully modified with SDS. After AO adsorption, the percentage of carbon was raised from  $72.36\%$  to  $80.09\%$  (Fig. 2b), this confirmed that AO has been successfully adsorbed by the adsorbent.

### 3.2. Optimization of AO adsorption variables

#### 3.2.1. Mathematical modeling and statistical analysis

The BBD approach was used to optimize the significant variables. Solution pH, dose of adsorbent, interaction time and dye initial concentrations are the major input variables that highly influence dyes adsorption capacity. Individual and joint effects of these parameters on the uptake capacity of PA-AC-SDS for AO were examined via statistically designed experiments. The complete design matrix and results of 29 experiments investigated by BBD for AO uptake are given in Table 3. Quadratic model was selected for describing and predicting AO adsorption onto PA-AC-SDS, as recommended by the software. The ultimate perceived model in terms of coded factors is given in Eq. (20).

$$Y = 281.69 + 17.05X_1 - 38.67X_2 + 33.61X_3 + 148.17X_4 + 10.22X_1X_3 + 14.87X_1X_4 - 17.87X_2X_4 + 38.30X_3X_4 - 76.34X_1^2 - 12.39X_2^2 - 29.96X_3^2 - 44.67X_4^2 \quad (20)$$

The positive and negative symbols in front of the expressions in Eq. (20) specify that these expressions synergistically and antagonistically affect the response, respectively [20]. Solution pH ( $X_1$ ), contact time ( $X_3$ ), initial concentration ( $X_4$ ), and the interaction parameters ( $X_1X_3$ ), ( $X_1X_4$ ) and ( $X_3X_4$ ) with positive coefficient have synergistic effect while adsorbent dose ( $X_2$ ), the interaction parameters ( $X_2X_4$ ), and quadratic parameters ( $X_1^2$ ), ( $X_2^2$ ), ( $X_3^2$ ), ( $X_4^2$ ) with negative coefficient have inhibitory effect on adsorption of AO.

For the model, the response coefficient was evaluated via multiple regression analysis. Statistical technique ANOVA was applied to assess the adequacy of the model applied and to observe the correlation among input parameters and responses. The  $F$ -values and probability  $p$ -values were utilized to estimate the importance of the model and of each model term. The ANOVA results for AO adsorption onto PA-AC-SDS are summarized in Table 4. The  $F$ -value of  $510.690$  and  $p$ -value of  $0.0001$  for the model showed it to be significant. The higher  $F$ -value of  $\text{prob} > F$



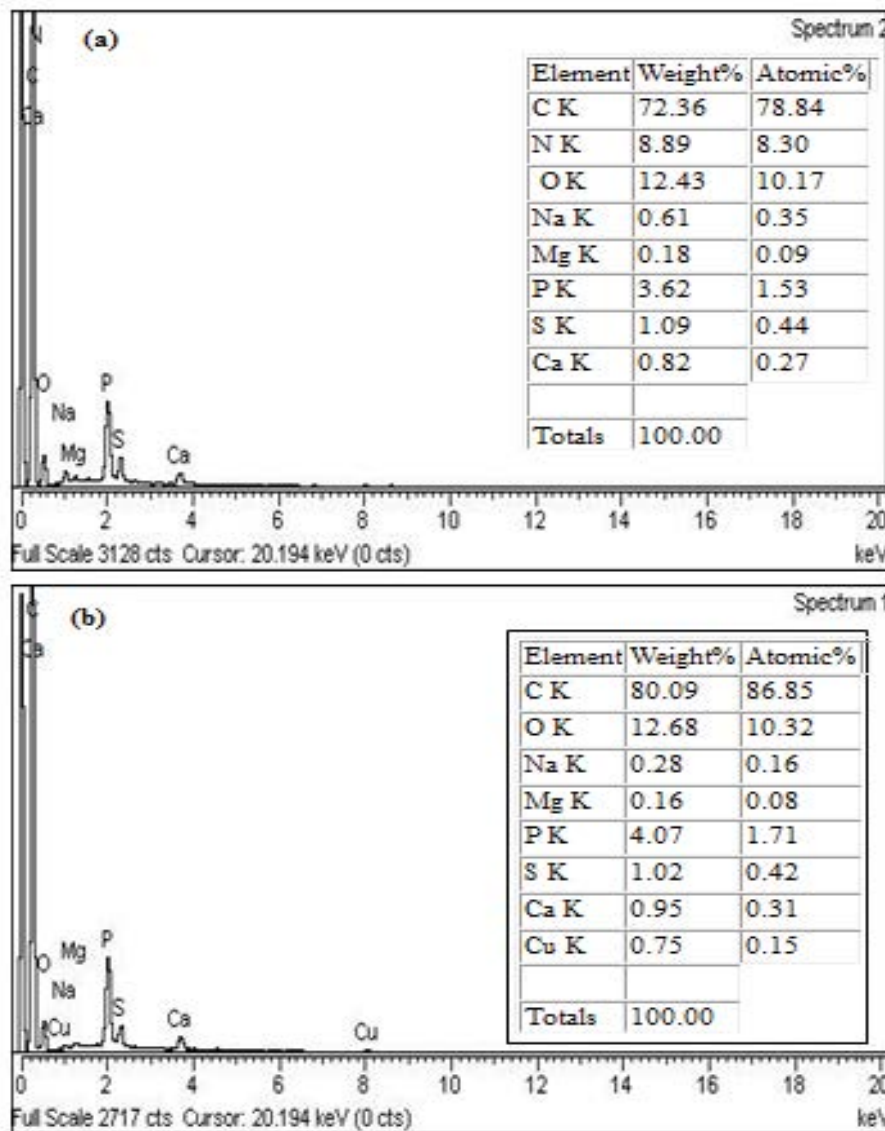


Fig. 2. EDX spectra and percentage of various elements determined from EDX analysis of PA-AC-SDS (a) before and (b) after adsorption.

less than 0.050 at 95% confidence level indicates that the model terms are significant. In the present research, the linear terms  $X_1, X_2, X_3, X_4$ , interaction parameters  $X_1X_3, X_1X_4, X_2X_4, X_3X_4$ , and quadratic parameters  $X_1^2, X_2^2, X_3^2, X_4^2$  are all significant model terms ( $p < 0.050$ ) and thus have considerable effect on the response under study. The insignificant model terms, such as  $X_1X_2, X_2X_3$  has negligible effect on the response and were excluded to improve the model.

Correlation coefficient  $R^2$ , AP which is signal to noise ratio that compare the range of the predicted values at the design points to the average prediction error, standard deviation (SD) and coefficient of variance (CV) were employed to evaluate the quality and validity of the model. Usually, a model with lower CV% and SD values is considered more precise. Moreover, there will be good agreement between the theoretical and experimental values of response for a model with higher  $R^2$  and AP ratio [52].

The  $R^2$  value for Eq. (20) was found to be 0.998, representing that the model can clarify 99.800% of the total deviation in response and only 0.20% cannot be elucidated. Also, the predicted  $R^2$  value (0.989) is in close association with the adjusted  $R^2$  value (0.9961). According to Vargas et al. [53], for best fitted model, the least value of  $R^2$  is 0.800. The closeness of  $R^2$  value to one and smaller SD (Table 4) provides the evidence that the developed quadratic model can accurately predict the response within the range of input variables. The diagnostic plots, such as plots of predicted vs. experimental values and normal probability plots of studentized residuals, were also used to scrutinize the fitness of the model (Fig. 3). The comparison between the model-predicted values based on Eq. (20) against experimental values (Fig. 3a) showed that the selected quadratic model can successfully explore the relationship among the input variable and the desired response. The normal

Table 4  
ANOVA and model summary statistics for response surface quadratic model for AO adsorption

Source	Sum of squares	Degree of freedom	Mean square	F-value	p-value Prob. > F	Comment
Model	3.520E+005	14	25,154.100	510.690	<0.0001	Significant
$X_1$	3,487.950	1	3,487.950	70.810	<0.0001	
$X_2$	17,940.950	1	17,940.950	364.240	<0.0001	
$X_3$	13,554.290	1	13,554.290	275.180	<0.0001	
$X_4$	2.630E+005	1	2.630E+005	5,348.660	<0.0001	
$X_1X_2$	8.970	1	8.970	0.180	0.676	
$X_1X_3$	417.610	1	417.610	8.480	0.0114	
$X_1X_4$	883.990	1	883.990	17.950	0.0008	
$X_2X_3$	41.890	1	41.890	0.850	0.0372	
$X_2X_4$	1,277.170	1	1,277.170	25.930	0.0002	
$X_3X_4$	5,867.190	1	5,867.190	119.120	<0.0001	
$X_1^2$	37,799.690	1	37,799.690	767.420	<0.0001	
$X_2^2$	995.570	1	995.570	20.210	0.0005	
$X_3^2$	5,823.580	1	5,823.580	118.230	<0.0001	
$X_4^2$	12,944.190	1	12,944.190	262.800	<0.0001	
Residual	689.570	14	49.260			
Lack of fit	689.350	10	68.940	1,232.300	0.0001	Significant
Pure error	0.220	4	0.056			
Cor. total	3.530E+005	28				

Model summary statistics						
Response (Y)	SD	CV (%)	R <sup>2</sup>	Adj. R <sup>2</sup>	Pred. R <sup>2</sup>	AP
$q_e$ (mg g <sup>-1</sup> ) AO	7.020	3.280	0.998	0.996	0.988	83.013

probability plot (Fig. 3b) displayed that all data points are linearly distributed and lying adjacent to a straight regression line indicate good fitting of the selected model. Fig. 3c also depicts the validation of the model in which the residuals are randomly distributed around the zero line. Furthermore, the reproducibility of the model was checked using coefficient of variance (CV). The CV value obtained for AO adsorption (Table 4) was less than 10% showing that the model is reproducible and reliable. AP, which is a measure of signal to noise ratio for the model, value higher than 4 is needed for acceptable signal [20]. In this case, the AP ratio for AO adsorption was found to be 83.010. This proved that the model has an adequate signal and can be applied to traverse the space defined by BBD.

### 3.2.2. Effects of process input variables

The ANOVA results and three dimensional (3D) response surface conspiracies were used to examine the main and combined effects of experimental input variables on AO adsorption by PA-AC-SDS. The 3D surface and contour plots were constructed for the substantial model (Eq. (20)) using Design-Expert software, in which two parameters were varied at a time, but the others were fixed at the center level (zero level). The ANOVA results (Table 4) shows that solution pH ( $X_1$ ), dosage adsorbent ( $X_2$ ), time of contact ( $X_3$ ) and dye initial concentration ( $X_4$ ) with  $p$ -value less than 0.0001, highly influence AO adsorption capacity. Similarly,

the quadratic effects of ( $X_1^2$ ), ( $X_2^2$ ), ( $X_3^2$ ), ( $X_4^2$ ) and interaction effects between ( $X_1X_3$ ), ( $X_1X_4$ ), ( $X_2X_4$ ) and ( $X_3X_4$ ) were also high due to larger  $F$ -value and lesser  $p$ -value ( $p < 0.050$ ).

Figs. 4a–f show 3D surface and contour plots, demonstrating the interaction effects of process variables on AO adsorption capacity. The interaction impact of pH ( $X_1$ ) and adsorbent dose ( $X_2$ ), keeping  $X_3$  and  $X_4$  fixed at zero level is shown in Fig. 4a. As can be seen, the AO uptake capacity is highly influenced by solution pH and was found to augment with raising pH up to 7.0. At lower pH, the active groups on PA-AC-SDS surface get protonated that enhances electrostatic repulsion amongst dye cations and positively charged adsorbent surface, which results in poorer AO adsorption. However, at low adsorbent dosage, the uptake capacity of AO increased with increasing solution pH until attaining the core value of 281.950 mg g<sup>-1</sup> at pH value near to 6.00. Beyond pH 7.50, the dye adsorption capacity starts to decrease again. This may be associated to SDS seeping from PA-AC-SDS at pH values beyond 7.50 that may lead to a pronounced drop in AO uptake capacity. Moreover, at pH value greater than  $pH_{pzc}$  ( $pH_{pzc} = 5.20$ ), the SDS polar heads bear greater negative charge that can interact with AO cations and thus lead to higher adsorption. Similar observations were made by Zolgharnein et al. [54] in the removal of brilliant green and crystal violet by surfactant-modified alumina. The uptake capacity has shown a decline trend with increasing adsorbent dosage. This may be due to adsorbent particles aggregation,

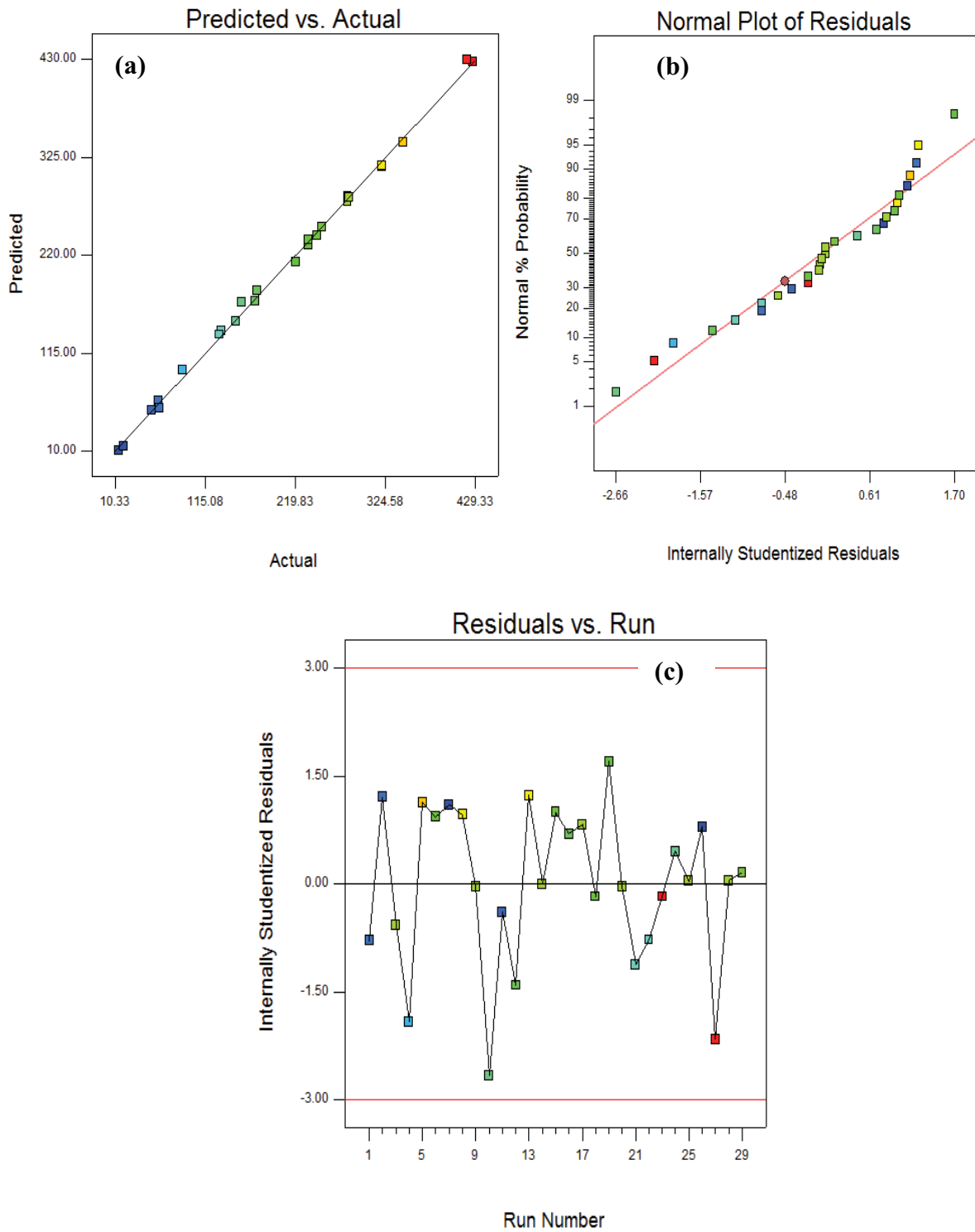


Fig. 3. Model validation diagnostic plots for AO adsorption (a) plot of predicted vs. actual values, (b) normal probability plot of studentized residuals and (c) studentized residual plots vs. run number.

resulting from high mass of PA-AC-SDS, which leads to a decrease in total surface area and availability of active sites for dye uptake [55]. Fig. 4b represents the interactive effect of pH ( $X_1$ ) and contact time ( $X_3$ ), keeping  $X_2$  and  $X_4$  at zero level ( $X_2 = 0.110$  g,  $X_4 = 550$  mg L<sup>-1</sup>). Both  $X_1$  and  $X_3$  have significant influence on dye adsorption capacity. AO uptake capacity goes up with increasing contact time and solution pH up to the optimum value. Initially AO adsorption was fast at the pH of about 6.00 due to the presence of more binding sites on PA-AC-SDS surface, which were then gradually decreased and almost reaches a constant value beyond 200 min. Maximum AO uptake (295.690 mg g<sup>-1</sup>) was achieved at pH of about 6.0 and contact

time of 240 min. The interactive effect of pH ( $X_1$ ) with dye initial concentration ( $X_4$ ) on AO uptake at constant  $X_2$  and  $X_3$  ( $X_2 = 0.11$  g,  $X_3 = 125$  min) is displayed in Fig. 4c. It was found that there is a significant interaction between pH and dye initial concentration for AO adsorption. At lower value of solution pH and initial concentration, AO has least uptake capacity (13.910 mg g<sup>-1</sup>). This behavior may be associated due to the electrostatic repulsion between dye cations and positively charged adsorbent surface caused by increased concentration of H<sup>+</sup> at low pH value. However, adsorption capacity increases with mounting initial dye concentration and solution pH up to the optimal value. This may be due to the improved driving force required to overcome the

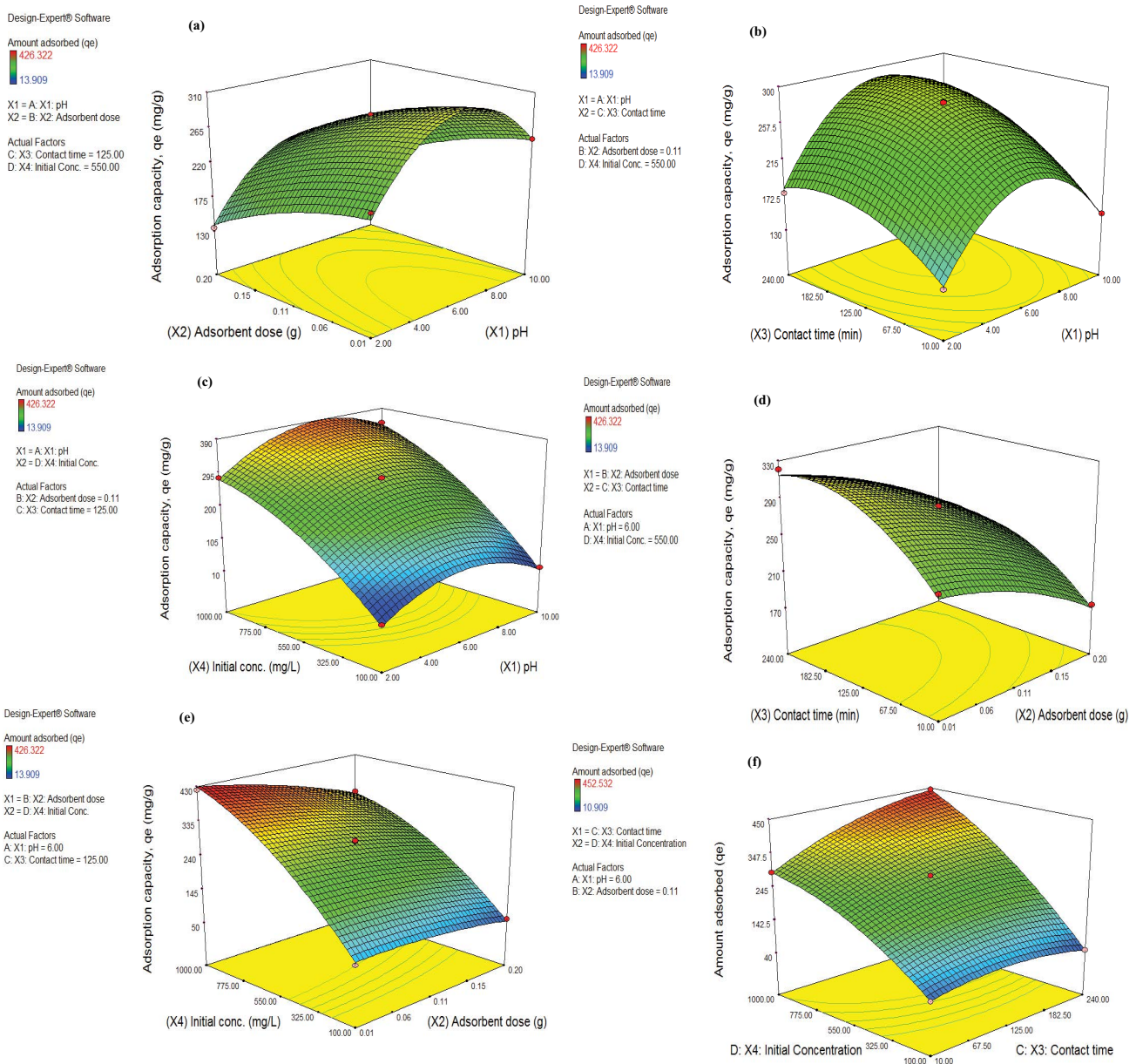


Fig. 4. Three-dimensional response surface and contour plots showing combined effects of (a) pH and adsorbent dose; (b) pH and contact time; (c) pH and dye initial concentration; (d) adsorbent dose and contact time; (e) adsorbent dose and dye initial concentration and (f) contact time and dye initial concentration on AO adsorption capacity.

mass transfer resistances that develop among dye species in solution phase and adsorbent surface. The increase in dye initial concentration causes the binding sites to be well surrounded and thus facilitates the diffusion of dye species inside adsorbent particles, which leads to high adsorption capacity. Marrakchi et al. [56] have similar findings for cationic dyes removal.

Fig. 4d illustrates cumulative effect of adsorbent dose ( $X_2$ ) and contact time ( $X_3$ ) at fixed  $X_1$  and  $X_4$  ( $X_1 = 6.00$ ,  $X_4 = 550 \text{ mg L}^{-1}$ ). The interaction effect of  $X_2$  and  $X_3$  does not influence AO uptake capacity significantly as evident from the small  $F$ -value of ANOVA analysis (Table 4). At lower adsorbent dosage, AO adsorption increases continuously with rising contact time and attains the peak value of approximately  $320.420 \text{ mg g}^{-1}$  at 240 min. This may be due to the fact that considerable amount of dye species will get diffused into the pores of adsorbent, thereby increasing the dye adsorption capacity. Fig. 4e shows the interactive effect of adsorbent dose ( $X_2$ ) and dye initial concentration ( $X_4$ ), keeping  $X_1$  and  $X_3$  at zero level ( $X_1 = 6.00$ ,  $X_3 = 125 \text{ min}$ ). It can be seen that the interaction effect of adsorbent dose and dye initial concentration significantly influences AO adsorption. Adsorption capacity increases with increasing dye initial concentration. Maximum AO uptake (around  $419.530 \text{ mg g}^{-1}$ ) was achieved at adsorbent dosage of almost  $0.010 \text{ g}$  and dye initial concentration of  $1,000 \text{ mg L}^{-1}$ . Fig. 4f signifies the combined effect of  $X_3$  and  $X_4$  at constant  $X_1$  and  $X_2$  ( $X_1 = 6.00$ ,  $X_2 = 0.11 \text{ g}$ ). It can be observed that AO uptake increases with time and dye initial concentration and accomplish the ultimate value of  $426.320 \text{ mg g}^{-1}$  beside the uppermost values of these variables. This phenomenon can be associated to the improved driving force between dye species in aqueous phase and PA-AC-SDS surface. Similar investigations have been reported by Ghasemi et al. [39] and Khodabandehloo et al. [57] for the uptake of Methylene blue using AC and *Salix babylonica* leaves as adsorbents.

### 3.2.3. Response optimization

The function of desirability, which may vary from 0.00 (undesirable) to 1.00 (highly desirable), was applied to optimize process variables and to achieve maximum adsorption capacity. Numerical optimization was used to find the best set of input variables at which highest uptake capacity for AO could be achieved. All the input variables were taken to be “within the range” and the goal was fixed as “maximum” to accomplish the response for AO with highest value and the desirability ramp obtained is shown in Fig. 5. Validation of the experimental model was carried out using the model predicted conditions. The optimum conditions predicted through this model were found to be solution pH ( $X_1$ ) of 6.00, adsorbent dosage of  $0.110 \text{ g}$ , agitation time of 240 min and AO initial concentration of  $1,000 \text{ mg L}^{-1}$  with 100% (1.0) desirability (Table 5). The adsorption capacity of AO predicted through this model was  $427.131 \text{ mg g}^{-1}$ , which was in good agreement with the experimentally determined value ( $425.060$ ) with minor error ( $-0.490\%$ ) between the actual and model predicted values. This indicates the precision and efficiency of the optimization method based on BBD.

### 3.2.4. Adsorption kinetic studies

The kinetic data of AO uptake at four different concentrations were scrutinized by pseudo-first-order, pseudo-second-order and Elovich models as shown in Figs. 6a–c, and values of the relevant parameters determined from the slope and intercept of the linear plots of Eqs. (5)–(7) are listed in Table 7. It could be seen from Figs. 6a and c that AO uptake by PA-AC-SDS could not be described well by pseudo-first-order and Elovich kinetic models throughout the sorption process and were valid only in the initial time intervals. Also, the smaller  $R^2$  values confirmed poorer fitting of these models. However, the plots of  $t/q_t$  vs.  $t$  for

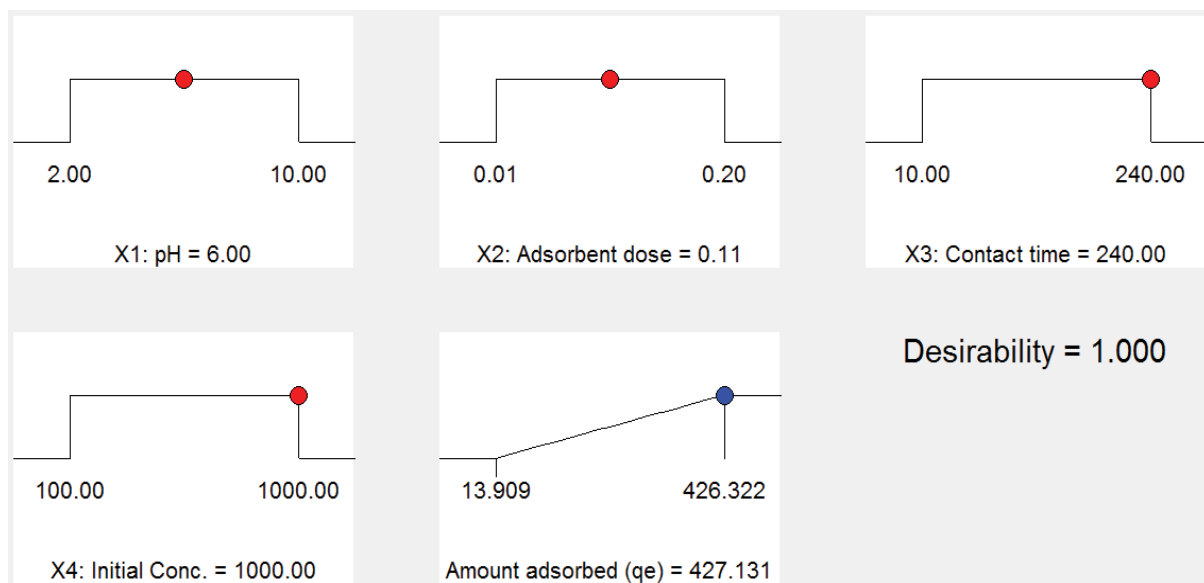


Fig. 5. Desirability ramp for numerical optimization of AO adsorption capacity.

pseudo-second-order kinetic model (Fig. 6b) were linear at all studied concentrations with  $R^2$  values of almost 1.00 (Table 7), indicating best fitting of pseudo-second-order rate equation to experimental data than pseudo-first-order and Elovich kinetic models. The uptake capacity calculated ( $q_{e,cal}$ ) from pseudo-second-order kinetic model agrees very well with the experimental values ( $q_{e,exp}$ ) as compared with pseudo-first-order model, suggesting that the pseudo-second-order model is much more better to elucidate AO adsorption by PA-AC-SDS at all the studied concentrations. It could also be seen from Table 6 which indicates that the values of rate constant ( $k_2$ ) falls with mounting AO initial concentration from 100 to 400 mg L<sup>-1</sup>. This decrease in adsorption rate at high initial concentration of AO could be ascribed to the higher competition among AO molecules for a limited number of adsorption sites on PA-AC-SDS surface [40]. But, the initial adsorption rate ( $h$ ) increased from 14.451 to 59.880 mg g<sup>-1</sup> min<sup>-1</sup> with increasing AO initial concentration from 100 to 400 mg L<sup>-1</sup>. The reason for this may be attributed to the increase in mass transport driving force originated by greater fractions of AO molecules to the existing binding sites on PA-AC-SDS surface. Ali et al. [42] and Daneshvar et al. [58] reported similar findings for malachite green adsorption onto H<sub>2</sub>O<sub>2</sub>-modified AC and methylene blue biosorption using modified macroalgae, respectively.

Intra-particle diffusion model was used to investigate the diffusion mechanism of AO adsorption by PA-AC-SDS. Fig. 6d depicts that the uptake of AO by PA-AC-SDS follows a three-stage process for all the initial concentrations.

The first stage signifies the rapid diffusion of AO molecules because of plenty of binding positions on PA-AC-SDS surface which is film diffusion controlled; the second stage represents the slow transport of AO within the pores, corresponding to intra-particle diffusion characterized by a diminution in slope. The third stage represents the equilibrium point, where the binding sites get saturated with AO molecules. The values of intra-particle diffusion model constants ( $k_{id}$  and C) as summarized in Table 7 show that intra-particle diffusion may be the rate-controlling step with  $k_{id,2}$  values for the second stages are smaller than  $k_{id,1}$  of the first stages for all initial concentrations of AO. The intercept values of C (Table 7) for the second stage were greater than that for the first stages and were found to increase with increasing AO initial concentrations; this suggests that the boundary layer effect augments with rising dye initial concentrations. The plots of  $q_t$  vs.  $t^{1/2}$  did not pass through the origin; this suggests that intra-particle diffusion alone is not the rate-limiting step. Many other pathways may also regulate AO uptake by PA-AC-SDS. Similar results have been reported by Shittu et al. [59] and Ali et al. [42] in the adsorption of Methylene blue by surfactant-functionalized graphitic carbon and malachite green by H<sub>2</sub>O<sub>2</sub>-modified AC, respectively.

To further confirm the mechanism of AO adsorption by PA-AC-SDS, whether it is controlled by film diffusion or intra-particle diffusion, Boyd model was applied to the experimental data. The values of function  $B_t$  were calculated using Eq. (10) and were plotted against  $t$  as demonstrated in Fig. 6e. In case,  $B_t$  against  $t$  plot is straight line with zero

Table 5

Model validation of AO adsorption, processes variable and response by Box–Behnken design of RSM

$X_1$ : pH	$X_2$ : Adsorbent dose (g)	$X_3$ : Contact time (min)	$X_4$ : Dye initial concentration (mg L <sup>-1</sup> )	AO adsorption capacity, $q_e$ (mg g <sup>-1</sup> )		Relative error (%)	Desirability
				Predicted	Experimental		
6.000	0.110	240.000	1,000.000	427.131	425.060	-0.490	1.000

Table 6

BET characterization, surface chemical properties and proximate–ultimate analysis of PA-AC-SDS

Textural properties							
$S_{BET}$ (m <sup>2</sup> g <sup>-1</sup> )	Micropore surface area (m <sup>2</sup> g <sup>-1</sup> )	Micropore volume (cm <sup>3</sup> g <sup>-1</sup> )	Mesopore volume (cm <sup>3</sup> g <sup>-1</sup> )	Total pore volume (cm <sup>3</sup> g <sup>-1</sup> )	Fraction, % (micropore)	Fraction, % (mesopore)	
1,114.390	665.540	0.440	0.380	0.820	53.660	46.340	
Acidic functional groups (mmol g <sup>-1</sup> )				Basic groups (mmol g)		pH <sub>PZC</sub>	
Carboxylic	Lactonic	Phenolic	Carbonyl	Total acidic groups			
1.010	0.840	0.720	0.240	2.810	0.290	5.200	
Proximate analysis (dry basis, wt.%)				Ultimate analysis (dry basis, wt.%)			
Moisture	Volatile	Ash	Fixed carbon	C	H	N	O
3.930	8.330	8.220	79.520	77.260	1.650	1.190	19.910

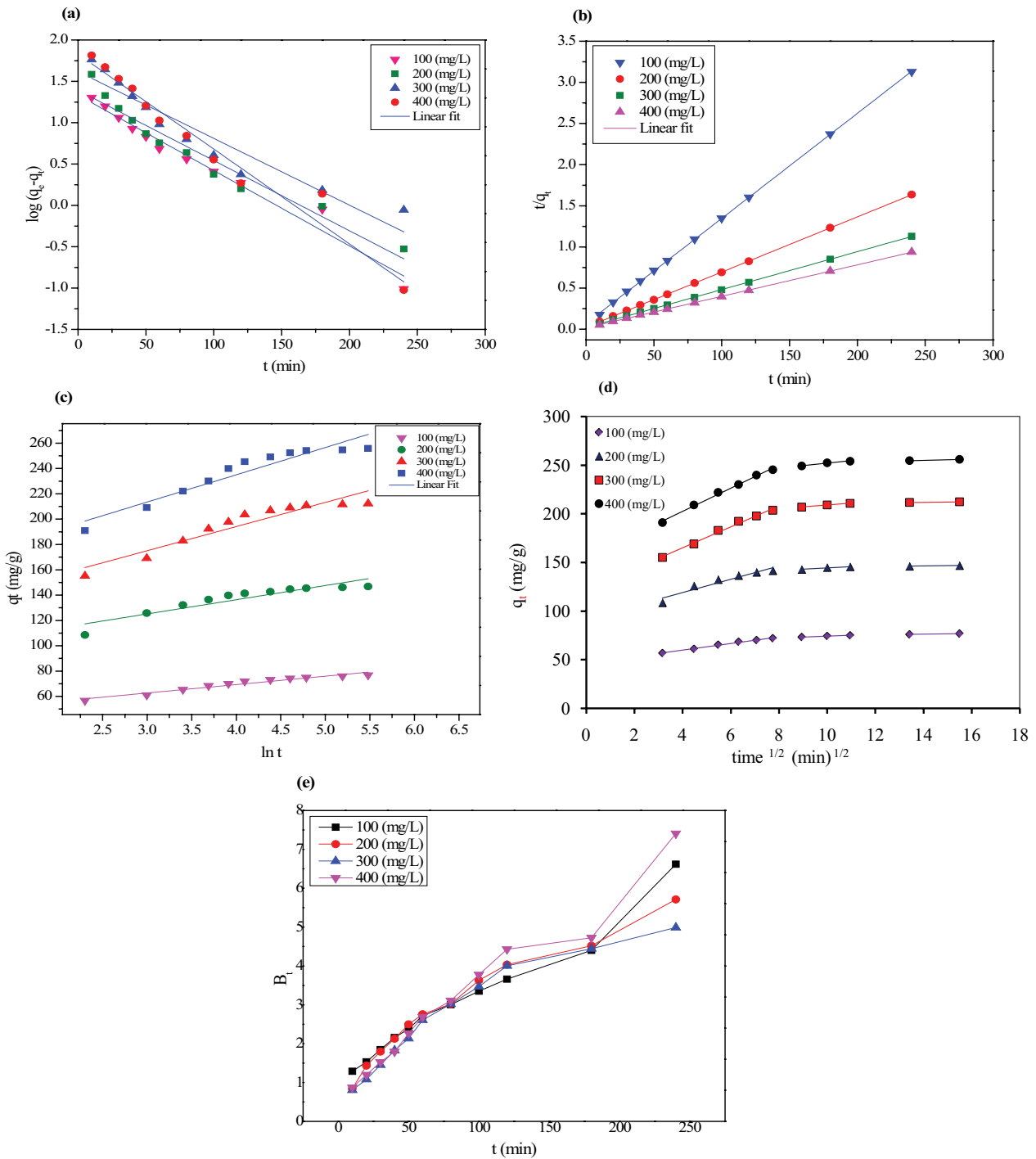


Fig. 6. Kinetics of AO adsorption by PA-AC-SDS (a) pseudo-first-order, (b) pseudo-second-order, (c) Elovich, (d) intra-particle diffusion and (e) Boyd model plots.

intercept shows that the sorption process is controlled by intra-particle diffusion, otherwise film diffusion will be the rate-limiting step [60]. As can be observed from Fig. 6e, the  $B_t$  vs.  $t$  plots are linear but did not pass through the origin, this demonstrates that film diffusion also plays a major role in the adsorption of AO by PA-AC-SDS in addition to particle diffusion. Similar investigations were made by other researchers for dye uptakes by various adsorbents [59,61,62].

### 3.2.5. Equilibrium isotherm studies

Adsorption isotherm examinations can be used to understand the correlation between the aqueous phase dye concentration at equilibrium point ( $C_e$ ) and quantity of dye adsorbed ( $q_e$ ) by a unit mass of adsorbent at a given temperature. Furthermore, the idea about the mechanism of adsorption, estimation of maximum uptake capacity and

Table 7

Kinetics and intra-particle diffusion model parameters for AO adsorption by PA-AC-SDS at 298 K with different initial dye concentrations

Model	Parameter	$C_0$ (mg L <sup>-1</sup> )			
		100	200	300	400
Pseudo-first-order	$q_{e,cal}$ (mg g <sup>-1</sup> )	21.538	24.620	41.438	67.344
	$k_1$ (10 <sup>-3</sup> ) (min <sup>-1</sup> )	20.957	19.575	18.650	26.484
	$R^2$	0.973	0.946	0.908	0.965
Pseudo-second-order	$q_{e,exp}$ (mg g <sup>-1</sup> )	76.798	147.025	213.145	256.011
	$q_{e,cal}$ (mg g <sup>-1</sup> )	78.125	149.254	217.391	263.158
	$k_2$ (10 <sup>-3</sup> ) (g mg <sup>-1</sup> min <sup>-1</sup> )	2.367	1.894	0.993	0.864
	$h$ (mg g <sup>-1</sup> min <sup>-1</sup> )	14.451	42.194	46.948	59.880
	$R^2$	0.999	1.000	0.999	0.999
Elovich	$\alpha$ (mg g <sup>-1</sup> min <sup>-1</sup> )	4,249.327	313.637	25.271	46.742
	$\beta \times 10^{-2}$ (g mg <sup>-1</sup> )	15.092	8.921	5.243	4.644
	$R^2$	0.947	0.857	0.903	0.911
Intra-particle diffusion	$k_{id,1}$ (mg g <sup>-1</sup> min <sup>-1</sup> )	3.404	6.896	10.777	11.927
	$C_1$ (mg g <sup>-1</sup> )	46.118	91.265	121.970	154.810
	$R_1^2$	0.993	0.923	0.992	0.994
	$k_{id,2}$ (mg g <sup>-1</sup> min <sup>-1</sup> )	0.872	1.384	1.971	2.553
	$C_2$ (mg g <sup>-1</sup> )	65.424	130.460	189.270	226.430
	$R_2^2$	0.991	0.954	0.996	0.975

surface properties of adsorbent can be obtained from isotherm model parameters [61,63].

As can be perceived from isotherms shape (Fig. 7a), which are L-type in the present case according to Giles et al.'s [64] classification, it can be suggested that for all temperatures, AO uptake capacity by PA-AC-SDS augments progressively with mounting dye initial concentration and finally reaches almost constant value at high AO concentration, which may represent high adsorbate–adsorbent interaction and monolayer formation of dye species on adsorbent surface. The increased adsorption with concentration can be associated to the mass transport driving force [65]. The isotherm curves given in Fig. 7a have also shown that AO uptake capacity increases with rising dye solution temperature from 293 to 323 K, which may be due to higher penetration of AO molecules into the micropores or formation of new binding positions on adsorbent surface at high temperatures [65]. The equilibrium data for AO adsorption were fitted to Langmuir, Freundlich, Temkin and D-R isotherm models as illustrated in Figs. 7b and e and the various isotherms parameters obtained from the slopes and intercepts of these plots are listed in Table 8. The fitting competency of the isotherm models was estimated from their regression coefficient ( $R^2$ ) values (Table 8), which was found to be higher for Langmuir and Temkin models. However, among these two, Langmuir model fitted very well with the adsorption data at all temperatures as obvious from the highest  $R^2$  values ( $R^2 > 0.993$ ) of  $C/q_e$  vs.  $C_e$  plots (Fig. 7b), which suggests monolayer coverage on homogeneous surface with identical sites. The  $R_L$  values for each of the different initial concentrations and temperatures lie between 0 and 1, which further confirmed that the adsorption processes of AO by PA-AC-SDS are favorable

and can be described very well via Langmuir isotherm model. Furthermore, the smaller  $1/n$  values (heterogeneity factor;  $1/n < 1$ ) of Freundlich model (Table 8) also supported favorable adsorption of AO by PA-AC-SDS at all temperatures. The mounting of adsorption energy ( $K_L$ ) and adsorption capacity ( $K_F$ ), obtained from Freundlich model (Table 8), with temperature reflects endothermic nature of AO adsorption by PA-AC-SDS. Similar results were observed by other investigators for dyes removal from wastewater [39,42,66,67]. The maximum uptake capacity (434.782 mg g<sup>-1</sup>) was higher than many other adsorbents previously investigated (Table 8); this shows that PA-AC-SDS could be an efficient adsorbent for detoxification of dyes bearing wastewater. The values of Temkin model constant  $b_T$  (associated to adsorption heat) and  $K_T$  (maximum binding energy) were correspondingly increased from 31.188 to 40.802 J mol<sup>-1</sup> and from 0.626 to 2.937 L mg<sup>-1</sup>, with rising temperature from 298 to 323 K. The increase in  $b_T$  and  $K_T$  values with temperature shows endothermic nature of adsorption process and improved electrostatic interaction between AO species and adsorbent surface [68]. The mean adsorption energy ( $E$ ), calculated via D-R model, was used to predict the mechanism of adsorption process, which was found to be less than 8.00 kJ mol<sup>-1</sup> at all temperatures (Table 8). This result suggested physisorption mechanism for AO adsorption by PA-AC-SDS [69].

### 3.2.6. Adsorption thermodynamics

The adsorption of AO onto PA-AC-SDS was scrutinized at different temperatures to calculate the various thermodynamic parameters such as enthalpy change ( $\Delta H^\circ$ ), entropy change ( $\Delta S^\circ$ ) and Gibb's free energy ( $\Delta G^\circ$ )



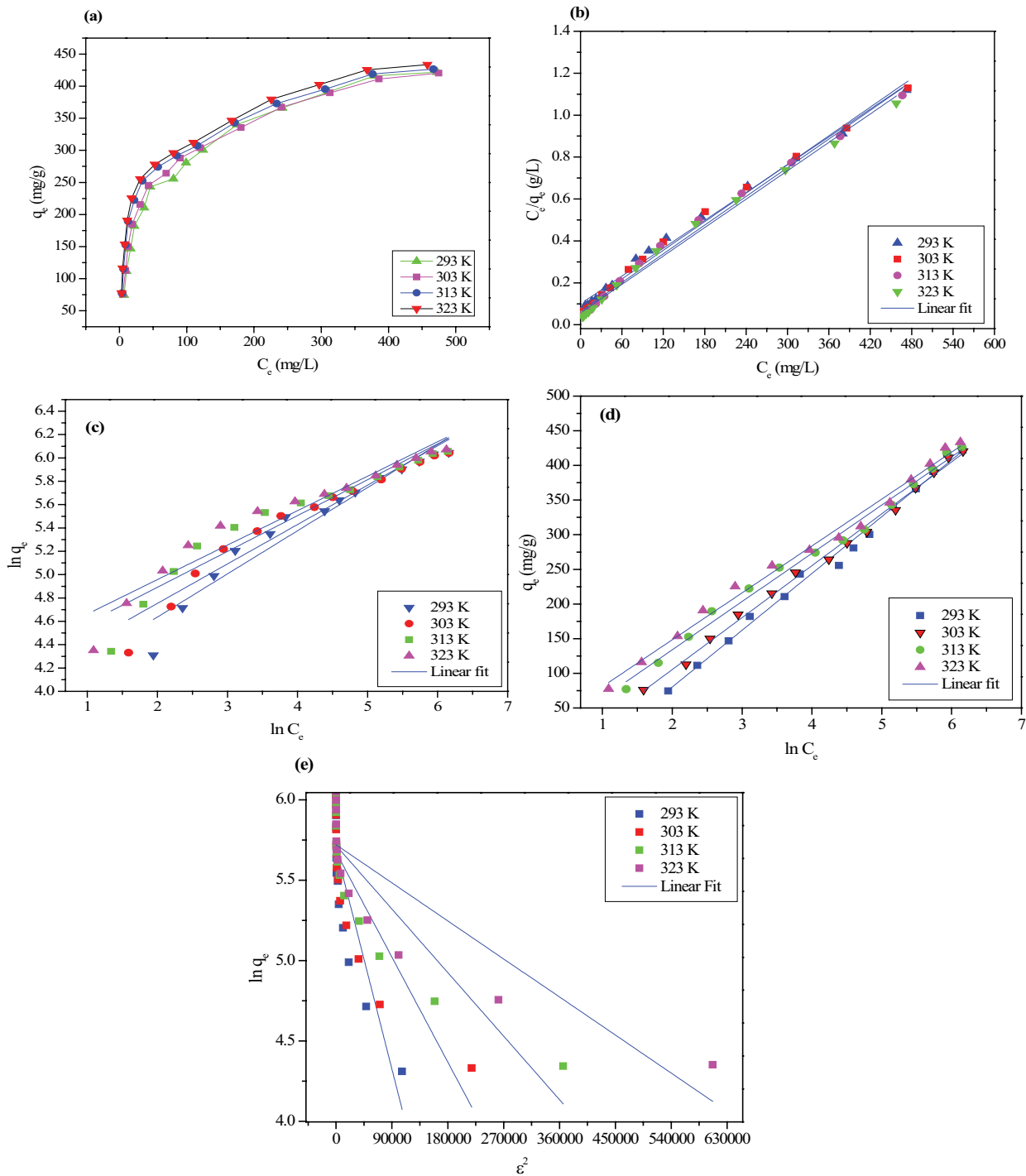


Fig. 7. (a) Adsorption equilibrium, (b) Langmuir, (c) Freundlich, (d) Temkin and (e) D-R isotherm model plots for AO adsorption onto PA-AC-SDS at different temperature.

as well as feasibility of uptake process. The values of these parameters were calculated using Eqs. (17) and (18) and the results obtained are listed in Table 9. The negative values of  $\Delta G^\circ$  show spontaneous and feasible adsorption of AO by PA-AC-SDS at all considered temperatures. The drop in  $\Delta G^\circ$  values with increase in temperature has shown that the adsorption process is energetically more viable at elevated

temperature. Positive  $\Delta H^\circ$  values presented endothermic nature of AO adsorption and the positive values of  $\Delta S^\circ$  suggested increased randomness at solid–solution interface, which represents good affinity of PA-AC-SDS for AO uptake under the given conditions. Similar investigations were made by other researchers for the removal of cationic dyes using different adsorbents materials [70–73].

Table 8  
Various isotherm constants for AO adsorption onto PA-AC-SDS at different temperatures

Isotherm	Parameters	Temperature (K)			
		293	303	313	323
Langmuir	$q_{\max, \text{exp}}$ (mg g <sup>-1</sup> )	420.285	422.018	426.670	433.681
	$q_{\max}$ (mg g <sup>-1</sup> )	434.782	434.782	434.782	434.782
	$K_L$ (L mg <sup>-1</sup> )	0.022	0.028	0.036	0.040
	$R^2$	0.993	0.994	0.993	0.993
	$R_L$	0.313	0.263	0.217	0.200
Freundlich	$K_F$ (mg g <sup>-1</sup> (L mg <sup>-1</sup> ) <sup>1/n</sup> )	49.264	59.063	72.060	78.831
	$1/n$	0.369	0.337	0.307	0.295
	$R^2$	0.944	0.945	0.926	0.931
Temkin	$K_T$ (L mg <sup>-1</sup> )	0.360	0.553	0.928	1.214
	$b_T$ (J mol <sup>-1</sup> )	29.726	33.629	33.398	39.690
	$R^2$	0.993	0.996	0.991	0.991
D-R	$q_{D-R}$ (mg g <sup>-1</sup> )	296.842	291.314	303.657	305.179
	$\beta$ (10 <sup>-6</sup> ) (mol <sup>2</sup> J <sup>-2</sup> )	15.208	7.256	4.393	2.633
	$E$ (kJ mol <sup>-1</sup> )	0.182	0.263	0.337	0.436
	$R^2$	0.753	0.699	0.761	0.743

### 3.2.7. Probable adsorption mechanism

The removal of AO by PA-AC-SDS involves different mechanisms, such as  $\pi$ - $\pi$  interactions, H-bonding, electrostatic interactions, film diffusion and pore filling as evident from FTIR analysis and mechanistic modeling of kinetics and isotherm data. PA-AC-SDS is a porous carbonaceous material having larger  $S_{\text{BET}}$  (1,114.390 m<sup>2</sup> g<sup>-1</sup>) and significant amount of mesopores (fraction of mesopore volume is 46.340%). This indicates that the mesopores might have assisted the diffusion of dye molecules into the adsorbent, which is supported by the intra-particle diffusion model (Fig. 6d) that pore filling may also play a major role in AO removal, as more than 45% adsorption achieved under pH 5.00. At pH value higher than 5.20, PA-AC-SDS surface is negatively charged due to the deprotonation of carboxylic (-COOH) and phenolic (C<sub>6</sub>H<sub>5</sub>OH) groups and also the presence of polar heads (SO<sub>3</sub><sup>-</sup>) from SDS and phosphonate anion (HPO<sub>3</sub><sup>-</sup>) on adsorbent surface can efficiently interact with dye cations in solution and leads to higher adsorption [54,74]. Therefore, the mechanism of AO uptake also involves electrostatic interaction supported by a remarkable increase in the dye adsorption capacity at pH = 6.00, which is higher than the pH<sub>PZC</sub> (pH<sub>PZC</sub> = 5.20) of adsorbent. Some of the dye molecules are thought to be removed by hydrophobic interaction between AO and nonpolar tail of SDS [59]. Before and after dye uptake, FTIR spectra of PA-AC-SDS (Fig. 1d) give clue about adsorption mechanism. The shift in the peak position for C=C from 1,562 cm<sup>-1</sup> toward higher wavenumber (1,584 cm<sup>-1</sup>) shows the involvement of  $\pi$ - $\pi$  interactions (or  $\pi$ - $\pi$  electron donor-acceptor interactions) among the  $\pi$ -electrons of dye aromatic rings and that of the  $\pi$ -electron rich sites on adsorbent surface [75]. Similarly, the band for -OH group around 3,327 cm<sup>-1</sup> shifted to higher wavenumber and a short intensity band at 3,335 cm<sup>-1</sup> shows the presence of H-bonding interactions

Table 9  
Thermodynamic parameters for adsorption of AO onto PA-AC-SDS at different temperatures

T (K)	$\Delta G^\circ$ (kJ mol <sup>-1</sup> )	$\Delta H^\circ$ (J mol <sup>-1</sup> )	$\Delta S^\circ$ (J mol <sup>-1</sup> K <sup>-1</sup> )
293	-6.884		
303	-7.119		
313	-7.355	16.153	23.550
323	-7.591		

between the hydrogen atom of -COOH and C<sub>6</sub>H<sub>5</sub>OH groups present on PA-AC-SDS surface and lone pairs of electrons on nitrogen atoms of dye molecules [76]. In addition, cation  $\pi$ -bonding amongst the protonated auxochrome (-C=N<sup>+</sup>H<sub>2</sub>) in dye molecules and the adsorbent  $\pi$ -electron enrich centers also play role in adsorption of AO by PA-AC-SDS. The most probable mechanism involved in the uptake of AO by PA-AC-SDS is illustrated in Fig. 8.

### 3.2.8. Desorption and regeneration study

Desorption tests were executed to examine the possible reuse of the dye-loaded sample. Desorption of AO from the surface of adsorbent (PA-AC-SDS) was studied by varying medium pH (2–12), eluents type (HCl, H<sub>2</sub>SO<sub>4</sub>, HNO<sub>3</sub>, EtOH, NaCl, NaOH and 5% (v/v) EtOH-HCl solution) and at different concentration of HCl (0.01–1.0 mol L<sup>-1</sup>) in batch mode and the results obtained are shown in Figs. 9a–c. It was found that these parameters have significant effect on AO desorption. As can be observed from Fig. 9a, AO desorption percentage increases with lowering medium pH and the highest desorption of 55.08% was achieved at pH 2.0. This shows that AO uptake by PA-AC-SDS may involve different sorts of electrostatic interactions among dye

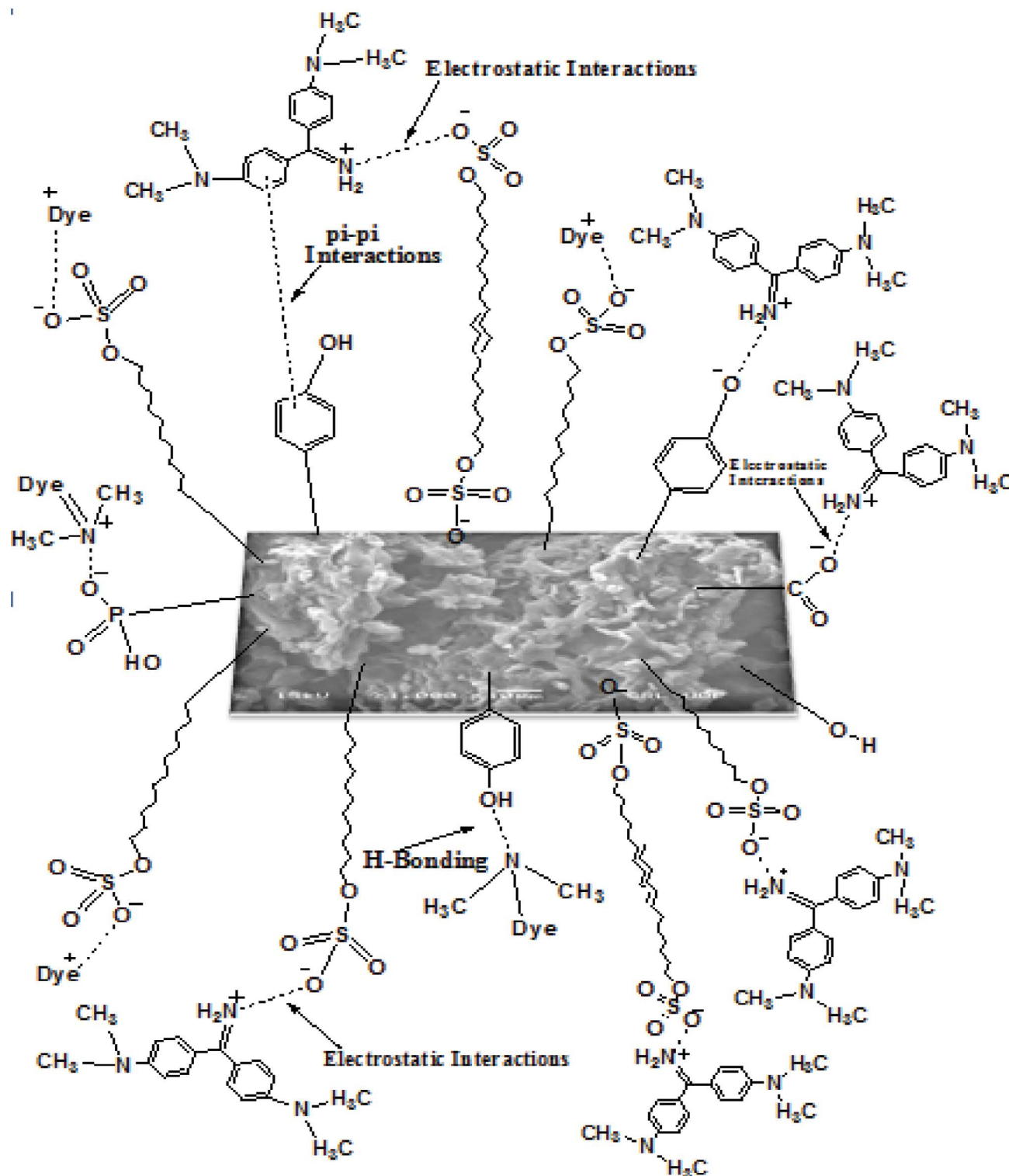


Fig. 8. Possible mechanism involved in the uptake of AO by PA-AC-SDS.

species and the functionalities on adsorbent surface [42,77]. Eluent type has more significant effect on AO desorption capacity as the dyes molecules are adhered to adsorbent surface by various types of attractive forces that can be weakened only by a specific eluent. In this study, maximum

elution (69.2%) was attained with 5% (v/v) EtOH-HCl solution, followed by the other eluents as evident from Fig. 9b. Therefore, 5% (v/v) EtOH-HCl solution was utilized for further regeneration studies. Similarly, effect of HCl concentrations on AO desorption was also explored. Desorption

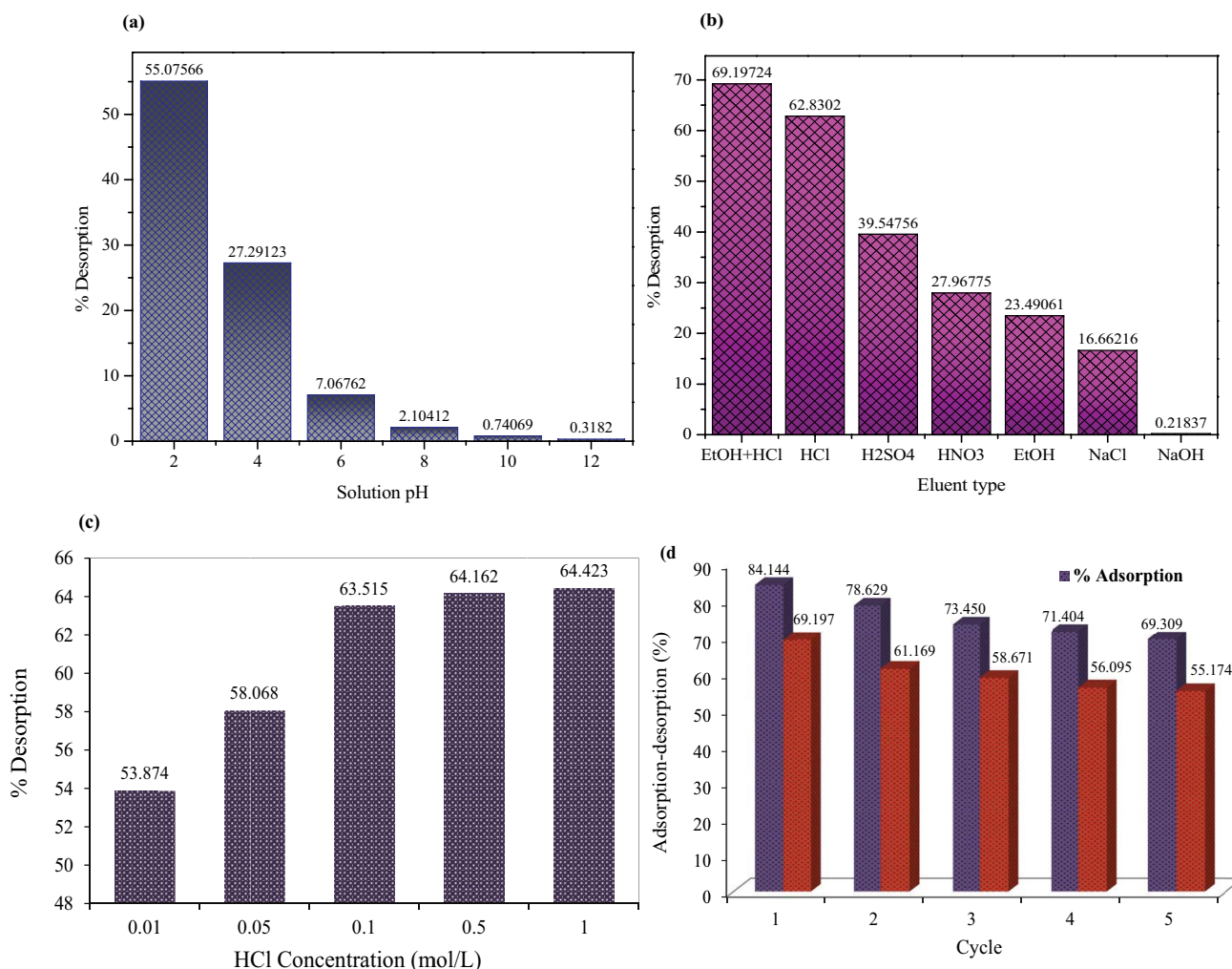


Fig. 9. Desorption of AO from PA-AC-SDS as a function of (a) medium pH, (b) eluents type, (c) HCl concentration and (d) regeneration and reusability of adsorbent using 5% (V/V) EtOH in 0.1 mol L<sup>-1</sup> HCl solution in five adsorption–desorption cycles.

percentage was observed to grow with increasing HCl concentration and optimum desorption (65.63%) was attained with 0.1 M HCl solution and no main change was detected beyond this value (Fig. 9c). The highest desorption in acidic conditions may be associated to the protonation of  $-\text{COOH}$  and  $\text{C}_6\text{H}_5\text{OH}$  groups on adsorbent surface that can facilitate release of dye cations. Oladipo and Gazi [78] observed similar results for crystal violet dye desorption using bentonite beads as adsorbent.

The cost effectiveness of sorption process was scrutinized via regeneration of the dye-loaded adsorbent in five successive adsorption–desorption cycles using 5% EtOH–HCl solution as eluent and the results obtained are given in Fig. 9d. The adsorption competency decreases after each cycle and a more prominent reduction of 10.69% was observed in the third cycle. Afterwards in the fourth and fifth cycles, no significant reduction was detected, which indicate that PA-AC-SDS could be recycled many times for detoxification of dyes bearing wastewater without any considerable loss in sorption capacity. The reduction in uptake efficiency in second and third cycles may be due to

damage of some active sites on PA-AC-SDS surface by acidic medium [79].

### 3.2.9. Performance evaluation

The maximum uptake capacity ( $q_{\text{max}}$ ) of PA-AC-SDS for AO was matched with different adsorbents reported in literature, as summarized in Table 10. It follows that PA-AC-SDS has significantly higher uptake capacity for AO than many reported adsorbents. This shows that modification of AC with anionic surfactant, SDS, can provide an adsorbent material that has high adsorption potential for cationic dyes such as AO removal from wastewater.

## 4. Conclusion

The SDS-modified activated carbon (PA-AC-SDS) was found to be an effective adsorbent for AO adsorption from aqueous systems. The modified AC was characterized by SEM, EDX, BET, FTIR, XRD, PZC and Boehm's titration

Table 10  
Comparison of maximum adsorption capacity ( $q_{\max}$ ) of AO uptake by PA-AC-HO with other adsorbents

Adsorbent	$q_{\max}$ (mg g <sup>-1</sup> )	References
AC loaded with ZnS:Cu	94.200	[80]
AC loaded with nano-particles (ZnS:Cu-NP-AC)	123.000	[80]
Gum xanthan-psyllium-cl-poly(acrylic acid-co-itaconic acid) based adsorbent	2.084	[81]
ZnO nanoparticles-loaded activated carbon (PES-PAC-ZnO-NPs)	48.78	[82]
PES-PAC	30.15	[82]
ZnO nanorod-activated carbon	88.500	[83]
Bi <sub>2</sub> S <sub>3</sub> -Ag <sub>2</sub> S-AC	202.43	[84]
ZnO:Cr-NPs-AC	211.6	[85]
Katira gum-cl-poly(acrylic acid-co-N,N-dimethylacrylamide) hydrogel [KG-cl-poly (AA-co-DMA)]	152.67	[86]
Brazil nut shells activated carbon (AC3-R2)	83	[87]
PA-AC-SDS	434.782	This study

analysis. The adsorbent has highly porous structure; good  $S_{\text{BET}}$  and appeared to be coated due to the dispersion of SDS as evident from a medium peak for sulfur in EDX spectrum. Boehm's titration results have shown that modification with SDS results in an increase in the content of basic groups from 0.130 to 0.290 mmol g<sup>-1</sup> on PA-AC-SDS surface relative to its precursor AC. Adsorption experiments were carried out to investigate the effect of four input variables such as solution pH, adsorbent dose, contact time and dye initial concentration on AO adsorption capacity using BBD of RSM. ANOVA showed adequate relationship between input variables and response (AO adsorption capacity). The  $F$ -values and  $p$ -values,  $R^2$  value and AP were used to determine the competence and fitting quality of the selected model and significance of input variables. Optimum conditions for AO adsorption with desirability of 1.00 has been found to be solution pH of 6.00, adsorbent dose of 0.110 g, contact time of 240 min and dye initial concentration of 1,000 mg/L, under which the experimentally determined uptake capacity was 425.060 mg g<sup>-1</sup>, which is in close agreement with the predicted value (427.130 mg g<sup>-1</sup>), with relative error of -0.49%. Kinetic investigations showed that the adsorption process could be controlled by the pseudo-second-order kinetic model. Moreover, intra-particle diffusion and Boyd's models verified that overall adsorption process was jointly controlled by film diffusion and intra-particle diffusion. The equilibrium data were fitted well the Langmuir model with maximum uptake capacity of 434.780 mg g<sup>-1</sup> and the values of separation factor ( $R_L$ ) lie between 0 and 1, showed that PA-AC-SDS could be an effective adsorbent for AO adsorption. The mechanisms that play a major role in the uptake process include H-bonding,  $\pi$ - $\pi$  interactions and electrostatic interactions. Thermodynamic studies showed spontaneous, feasible and endothermic nature of AO adsorption onto PA-AC-SDS under the studied conditions. Desorption studies showed good regeneration capacity of PA-AC-SDS that make it an economic and effective adsorbent for treatment of dyes-containing aqueous systems.

### Acknowledgments

The authors gratefully acknowledge the financial support and facilities provided by the National Center of Excellence

in Physical Chemistry, University of Peshawar, Pakistan, for completing this research project.

### References

- [1] E.N. Zare, A. Motahari, M. Sillanpää, Nanoadsorbents based on conducting polymer nanocomposites with main focus on polyaniline and its derivatives for removal of heavy metal ions/dyes: a review, *Environ. Res.*, 162 (2018) 173–195.
- [2] A.A. Basheer, New generation nano-adsorbents for the removal of emerging contaminants in water, *J. Mol. Liq.*, 261 (2018) 583–593.
- [3] Y. Dai, Q. Sun, W. Wang, L. Lu, M. Liu, J. Li, S. Yang, Y. Sun, K. Zhang, J. Xu, Utilizations of agricultural waste as adsorbent for the removal of contaminants: a review, *Chemosphere*, 211 (2018) 235–253.
- [4] I. Mironyuk, T. Tatarchuk, M. Naushad, H. Vasylyeva, I. Mykytyn, Highly efficient adsorption of strontium ions by carbonated mesoporous TiO<sub>2</sub>, *J. Mol. Liq.*, 285 (2019) 742–753.
- [5] L. Deng, H. Zeng, Z. Shi, W. Zhang, J. Luo, Sodium dodecyl sulfate intercalated and acrylamide anchored layered double hydroxides: a multifunctional adsorbent for highly efficient removal of Congo red, *J. Colloid Interface Sci.*, 521 (2018) 172–182.
- [6] M. Naushad, A.A. Alqadami, Z.A. AlOthman, I.H. Alsohaimi, M.S. Algami, A.M. Aldawsari, Adsorption kinetics, isotherm and reusability studies for the removal of cationic dye from aqueous medium using arginine modified activated carbon, *J. Mol. Liq.*, 293 (2019) 111442.
- [7] International Agency For Research On Cancer, Overall evaluations of carcinogenicity: and updating of IARC monographs, vol. 1 to 42. IARC monographs on the evaluation of the carcinogenic risk of chemicals to humans: Suppl 7, IARC, 7 (1987) 1–440.
- [8] W.-f. Chen, L. Pan, L.-f. Chen, Z. Yu, Q. Wang, C.-c. Yan, Comparison of EDTA and SDS as potential surface impregnation agents for lead adsorption by activated carbon, *Appl. Surf. Sci.*, 309 (2014) 38–45.
- [9] F. Golmohammadi, M. Hazrati, M. Safari, Removal of reactive yellow 15 from water sample using a magnetite nanoparticles coated with covalently immobilized dimethyl octadecyl [3-(trimethoxysilylpropyl)] ammonium chloride ionic liquid, *Microchem. J.*, 144 (2019) 64–72.
- [10] M. Naushad, G. Sharma, Z.A. AlOthman, Photodegradation of toxic dye using Gum Arabic-crosslinked-poly (acrylamide)/Ni(OH)<sub>2</sub>/FeOOH nanocomposites hydrogel, *J. Cleaner Prod.*, 241 (2019) 118263.
- [11] A. Hassani, L. Alidokht, A. Khataee, S. Karaca, Optimization of comparative removal of two structurally different basic dyes using coal as a low-cost and available adsorbent, *Taiwan Inst. Chem. Eng.*, 45 (2014) 1597–1607.

- [12] C.K. Ahn, D. Park, S.H. Woo, J.M. Park, Removal of cationic heavy metal from aqueous solution by activated carbon impregnated with anionic surfactants, *J. Hazard. Mater.*, 164 (2009) 1130–1136.
- [13] J. Mohanraj, D. Durgalakshmi, S. Balakumar, P. Aruna, S. Ganesan, S. Rajendran, M. Naushad, Low cost and quick time absorption of organic dye pollutants under ambient condition using partially exfoliated graphite, *J. Water Process Eng.*, 34 (2019) 101078.
- [14] W. Lee, S. Yoon, J.K. Choe, M. Lee, Y. Choi, Anionic surfactant modification of activated carbon for enhancing adsorption of ammonium ion from aqueous solution, *Sci. Total Environ.*, 639 (2018) 1432–1439.
- [15] M. Nadeem, M. Shabbir, M. Abdullah, S. Shah, G. McKay, Sorption of cadmium from aqueous solution by surfactant-modified carbon adsorbents, *Chem. Eng. J.*, 148 (2009) 365–370.
- [16] M. Foroughi-dahr, H. Abolghasemi, M. Esmaili, G. Nazari, B. Rasem, Experimental study on the adsorptive behavior of Congo red in cationic surfactant-modified tea waste, *Process Saf. Environ. Prot.*, 95 (2015) 226–236.
- [17] P. Janoš, V. Šmidová, Effects of surfactants on the adsorptive removal of basic dyes from water using an organomineral sorbent—iron humate, *J. Colloid Interface Sci.*, 291 (2005) 19–27.
- [18] X.-I. Song, M.-w. Zhang, Y. Zhang, S.-T. Huang, B.-Y. Geng, R.-B. Meng, Y.-Z. Yang, Y.-S. Zhong, H.-Y. Liu, Surface modification of coconut-based activated carbon by SDS and its effects on Pb<sup>2+</sup> adsorption, *J. Cent. South Univ.*, 20 (2013) 1156–1160.
- [19] S. Moradi, Microwave assisted preparation of sodium dodecyl sulphate (SDS) modified ordered nanoporous carbon and its adsorption for MB dye, *J. Ind. Eng. Chem.*, 20 (2014) 208–215.
- [20] A. Asfaram, M. Ghaedi, M.H.A. Azghandi, A. Goudarzi, S. Hajati, Ultrasound-assisted binary adsorption of dyes onto Mn@ CuS/ZnS-NC-AC as a novel adsorbent: application of chemometrics for optimization and modeling, *J. Ind. Eng. Chem.*, 54 (2017) 377–388.
- [21] T. Mahmood, R. Ali, A. Naeem, M. Hamayun, M. Aslam, Potential of used *Camellia sinensis* leaves as precursor for activated carbon preparation by chemical activation with H<sub>3</sub>PO<sub>4</sub>; optimization using response surface methodology, *Process Saf. Environ. Prot.*, 109 (2017) 548–563.
- [22] E.P. Barrett, L.G. Joyner, P.P. Halenda, The determination of pore volume and area distributions in porous substances. I. Computations from nitrogen isotherms, *J. Am. Chem. Soc.*, 73 (1951) 373–380.
- [23] F. Rodriguez-Reinoso, M. Molina-Sabio, M. Gonzalez, The use of steam and CO<sub>2</sub> as activating agents in the preparation of activated carbons, *Carbon*, 33 (1995) 15–23.
- [24] G.D. Vyavahare, R.G. Gurav, P.P. Jadhav, R.R. Patil, C.B. Aware, J.P. Jadhav, Response surface methodology optimization for sorption of malachite green dye on sugarcane bagasse biochar and evaluating the residual dye for phyto and cytogenotoxicity, *Chemosphere*, 194 (2018) 306–315.
- [25] A.M. Ghaedi, S. Karamipour, A. Vafaei, M.M. Baneshi, V. Kiarostami, Optimization and modeling of simultaneous ultrasound-assisted adsorption of ternary dyes using copper oxide nanoparticles immobilized on activated carbon using response surface methodology and artificial neural network, *Ultrason. Sonochem.*, 51 (2019) 264–280.
- [26] Z.N. Garba, A.A. Rahim, Process optimization of K<sub>2</sub>C<sub>2</sub>O<sub>4</sub>-activated carbon from *Prosopis africana* seed hulls using response surface methodology, *J. Anal. Appl. Pyrol.*, 107 (2014) 306–312.
- [27] D.C. Montgomery, *Design and Analysis of Experiments*, John Wiley & Sons, 2017.
- [28] S.K. Lagergren, About the theory of so-called adsorption of soluble substances, *K. Sven. Vetenskapskad. Handl.*, 24 (1898) 1–39.
- [29] Y.-S. Ho, G. McKay, Pseudo-second order model for sorption processes, *Process Biochem.*, 34 (1999) 451–465.
- [30] J. Gülen, B. Akin, M. Özgür, Ultrasonic-assisted adsorption of methylene blue on sumac leaves, *Desal. Water Treat.*, 57 (2016) 9286–9295.
- [31] G. Manikandan, S. Kumar, A. Saravanan, Modelling and analysis on the removal of methylene blue dye from aqueous solution using physically/chemically modified *Ceiba pentandra* seeds, *J. Ind. Eng. Chem.*, 62 (2018) 446–461.
- [32] W.J. Weber, J.C. Morris, Kinetics of adsorption on carbon from solution, *J. Sanit. Eng. Div.*, 89 (1963) 31–60.
- [33] G. Boyd, A. Adamson, L. Myers Jr, The exchange adsorption of ions from aqueous solutions by organic zeolites. II. Kinetics, *J. Am. Chem. Soc.*, 69 (1947) 2836–2848.
- [34] I. Langmuir, The constitution and fundamental properties of solids and liquids. Part I. Solids, *J. Am. Chem. Soc.*, 38 (1916) 2221–2295.
- [35] H. Freundlich, Über die adsorption in lösungen, *Z. Phys. Chem.*, 57 (1907) 385–470.
- [36] M. Temkin, V. Pyzhev, Recent modifications to Langmuir isotherms, *Acta Physicochim URSS*, 12 (1940) 217–225.
- [37] M. Dubinin, The equation of the characteristic curve of activated charcoal, *Dokl. Akad. Nauk. SSSR.*, 55 (1947) 327–329.
- [38] T. Weber, Chakravorti, Pore and solid diffusion models for fixed-bed adsorbers, *AIChE J.*, 20 (1974) 228–238.
- [39] M. Ghasemi, S. Mashhadi, M. Asif, I. Tyagi, S. Agarwal, V.K. Gupta, Microwave-assisted synthesis of tetraethylene pentamine functionalized activated carbon with high adsorption capacity for Malachite green dye, *J. Mol. Liq.*, 213 (2016) 317–325.
- [40] Z. Cheng, L. Zhang, X. Guo, X. Jiang, T. Li, Adsorption behavior of direct red 80 and congo red onto activated carbon/surfactant: process optimization, kinetics and equilibrium, *Spectrochim. Acta Part A*, 137 (2015) 1126–1143.
- [41] M.R. Malekbala, M.A. Khan, S. Hosseini, L.C. Abdullah, T.S. Choong, Adsorption/desorption of cationic dye on surfactant modified mesoporous carbon coated monolith: equilibrium, kinetic and thermodynamic studies, *J. Ind. Eng. Chem.*, 21 (2015) 369–377.
- [42] R. Ali, T. Mahmood, S.U. Din, A. Naeem, M. Aslam, M. Farooq, Efficient removal of hazardous malachite green dye from aqueous solutions using H<sub>2</sub>O<sub>2</sub> modified activated carbon as potential low-cost adsorbent: kinetic, equilibrium, and thermodynamic studies, *Desal. Water Treat.*, 151 (2019) 167–182.
- [43] A. Gallardo-Moreno, C. González-García, M. Gonzalez-Martín, J. Bruque, Arrangement of SDS adsorbed layer on carbonaceous particles by zeta potential determinations, *Colloids Surf. A*, 249 (2004) 57–62.
- [44] E. El-Shafey, S.N. Ali, S. Al-Busafi, H.A. Al-Lawati, Preparation and characterization of surface functionalized activated carbons from date palm leaflets and application for methylene blue removal, *J. Environ. Chem. Eng.*, 4 (2016) 2713–2724.
- [45] E.G. Lemraski, S. Sharafinia, Kinetics, equilibrium and thermodynamics studies of Pb<sup>2+</sup> adsorption onto new activated carbon prepared from Persian mesquite grain, *J. Mol. Liq.*, 219 (2016) 482–492.
- [46] Q. Sun, R.G. Saratale, G.D. Saratale, D.-S. Kim, Pristine and modified radix *Angelicae dahuricae* (Baizhi) residue for the adsorption of methylene blue from aqueous solution: a comparative study, *J. Mol. Liq.*, 265 (2018) 36–45.
- [47] R.M. Novais, A.P. Caetano, M.P. Seabra, J.A. Labrincha, R.C. Pullar, Extremely fast and efficient methylene blue adsorption using eco-friendly cork and paper waste-based activated carbon adsorbents, *J. Cleaner Prod.*, 197 (2018) 1137–1147.
- [48] P. Pal, A. Pal, Surfactant-modified chitosan beads for cadmium ion adsorption, *Int. J. Biol. Macromol.*, 104 (2017) 1548–1555.
- [49] L. Zhao, L. Gao, Coating multi-walled carbon nanotubes with zinc sulfide, *J. Mater. Chem.*, 14 (2004) 1001–1004.
- [50] X. Wei, Z. Wu, C. Du, Z. Wu, B.-C. Ye, G. Cravotto, Enhanced adsorption of atrazine on a coal-based activated carbon modified with sodium dodecyl benzene sulfonate under microwave heating, *J. Taiwan Inst. Chem. Eng.*, 77 (2017) 257–262.
- [51] H. Guedidi, L. Reinert, J.-M. Lévêque, Y. Soneda, N. Bellakhal, L. Duclaux, The effects of the surface oxidation of activated

- carbon, the solution pH and the temperature on adsorption of ibuprofen, *Carbon*, 54 (2013) 432–443.
- [52] F. Ansari, M. Ghaedi, M. Taghdiri, A. Asfaram, Application of ZnO nanorods loaded on activated carbon for ultrasonic assisted dyes removal: experimental design and derivative spectrophotometry method, *Ultrason. Sonochem.*, 33 (2016) 197–209.
- [53] A.M. Vargas, A.C. Martins, V.C. Almeida, Ternary adsorption of acid dyes onto activated carbon from flamboyant pods (*Delonix regia*): analysis by derivative spectrophotometry and response surface methodology, *Chem. Eng. J.*, 195 (2012) 173–179.
- [54] J. Zolgharnein, M. Bagtash, T. Shariatmanesh, Simultaneous removal of binary mixture of Brilliant Green and Crystal Violet using derivative spectrophotometric determination, multivariate optimization and adsorption characterization of dyes on surfactant modified nano- $\gamma$ -alumina, *Spectrochim. Acta Part A*, 137 (2015) 1016–1028.
- [55] M. Goswami, P. Phukan, Enhanced adsorption of cationic dyes using sulfonic acid modified activated carbon, *J. Environ. Chem. Eng.*, 5 (2017) 3508–3517.
- [56] F. Marrakchi, M. Auta, W. Khanday, B. Hameed, High-surface-area and nitrogen-rich mesoporous carbon material from fishery waste for effective adsorption of methylene blue, *Powder Technol.*, 321 (2017) 428–434.
- [57] A. Khodabandehloo, A. Rahbar-Kelishami, H. Shayesteh, Methylene blue removal using *Salix babylonica* (Weeping willow) leaves powder as a low-cost biosorbent in batch mode: kinetic, equilibrium, and thermodynamic studies, *J. Mol. Liq.*, 244 (2017) 540–548.
- [58] E. Daneshvar, A. Vazirzadeh, A. Niazi, M. Sillanpää, A. Bhatnagar, A comparative study of methylene blue biosorption using different modified brown, red and green macroalgae—effect of pretreatment, *Chem. Eng. J.*, 307 (2017) 435–446.
- [59] I. Shittu, A.A. Edathil, A. Alsaeedi, S. Al-Asheh, K. Polychronopoulou, F. Banat, Development of novel surfactant functionalized porous graphitic carbon as an efficient adsorbent for the removal of methylene blue dye from aqueous solutions, *J. Water Process Eng.*, 28 (2019) 69–81.
- [60] S. Kaur, S. Rani, R. Mahajan, M. Asif, V.K. Gupta, Synthesis and adsorption properties of mesoporous material for the removal of dye safranin: kinetics, equilibrium, and thermodynamics, *J. Ind. Eng. Chem.*, 22 (2015) 19–27.
- [61] M. Ghaedi, A. Ansari, M. Habibi, A. Asghari, Removal of malachite green from aqueous solution by zinc oxide nanoparticle loaded on activated carbon: kinetics and isotherm study, *J. Ind. Eng. Chem.*, 20 (2014) 17–28.
- [62] M.A. Ahmad, N.K. Rahman, Equilibrium, kinetics and thermodynamic of Remazol Brilliant Orange 3R dye adsorption on coffee husk-based activated carbon, *Chem. Eng. J.*, 170 (2011) 154–161.
- [63] A. Asfaram, M. Ghaedi, S. Agarwal, I. Tyagi, V.K. Gupta, Removal of basic dye Auramine-O by ZnS: Cu nanoparticles loaded on activated carbon: optimization of parameters using response surface methodology with central composite design, *RSC Adv.*, 5 (2015) 18438–18450.
- [64] C.H. Giles, D. Smith, A. Huitson, A general treatment and classification of the solute adsorption isotherm. I. Theoretical, *J. Colloid Interface Sci.*, 47 (1974) 755–765.
- [65] H. Laksaci, A. Khelifi, B. Belhamdi, M. Trari, The use of prepared activated carbon as adsorbent for the removal of orange G from aqueous solution, *Microchem. J.*, 145 (2019) 908–913.
- [66] P. Rai, R.K. Gautam, S. Banerjee, V. Rawat, M. Chattopadhyaya, Synthesis and characterization of a novel SnFe<sub>2</sub>O<sub>4</sub>@ activated carbon magnetic nanocomposite and its effectiveness in the removal of crystal violet from aqueous solution, *J. Environ. Chem. Eng.*, 3 (2015) 2281–2291.
- [67] Y.-D. Liang, Y.-J. He, T.-T. Wang, L.-H. Lei, Adsorptive removal of gentian violet from aqueous solution using CoFe<sub>2</sub>O<sub>4</sub>/activated carbon magnetic composite, *J. Water Process Eng.*, 27 (2019) 77–88.
- [68] A. Jalil, S. Triwahyono, M. Yaakob, Z. Azmi, N. Sapawe, N. Kamarudin, H. Setiabudi, N. Jaafar, S. Sidik, S. Adam, Utilization of bivalve shell-treated *Zea mays* L. (maize) husk leaf as a low-cost biosorbent for enhanced adsorption of malachite green, *Bioresour. Technol.*, 120 (2012) 218–224.
- [69] C. Muthukumaran, V.M. Sivakumar, M. Thirumarimurugan, Adsorption isotherms and kinetic studies of crystal violet dye removal from aqueous solution using surfactant modified magnetic nanoadsorbent, *J. Taiwan Inst. Chem. Eng.*, 63 (2016) 354–362.
- [70] P. Pal, A. Pal, Dye removal using waste beads: efficient utilization of surface-modified chitosan beads generated after lead adsorption process, *J. Water Process Eng.*, 31 (2019) 100882.
- [71] N.A. El Essawy, S.M. Ali, H.A. Farag, A.H. Konsowa, M. Elnouby, H.A. Hamad, Green synthesis of graphene from recycled PET bottle wastes for use in the adsorption of dyes in aqueous solution, *Ecotoxicol. Environ. Saf.*, 145 (2017) 57–68.
- [72] A. Salima, B. Benaouda, B. Noureddine, L. Duclaux, Application of *Ulva lactuca* and *Systoceira stricta* algae-based activated carbons to hazardous cationic dyes removal from industrial effluents, *Water Res.*, 47 (2013) 3375–3388.
- [73] J. Gülen, Z. Altın, M. Özgür, Removal of amitraz from aqueous solutions on clay by adsorption technique at industrial scale, *Mater. Test.*, 59 (2017) 94–100.
- [74] T.B. Pushpa, J. Vijayaraghavan, S.S. Basha, V. Sekaran, K. Vijayaraghavan, J. Jegan, Investigation on removal of malachite green using EM based compost as adsorbent, *Ecotoxicol. Environ. Saf.*, 118 (2015) 177–182.
- [75] H.N. Tran, S.-J. You, H.-P. Chao, Fast and efficient adsorption of methylene green 5 on activated carbon prepared from new chemical activation method, *J. Environ. Manage.*, 188 (2017) 322–336.
- [76] L. Zhang, H. Zhang, W. Guo, Y. Tian, Removal of malachite green and crystal violet cationic dyes from aqueous solution using activated sintering process red mud, *Appl. Clay Sci.*, 93 (2014) 85–93.
- [77] E. Daneshvar, A. Vazirzadeh, A. Niazi, M. Kousha, M. Naushad, A. Bhatnagar, Desorption of Methylene blue dye from brown macroalgae: effects of operating parameters, isotherm study and kinetic modeling, *J. Cleaner Prod.*, 152 (2017) 443–453.
- [78] A.A. Oladipo, M. Gazi, Enhanced removal of crystal violet by low cost alginate/acid activated bentonite composite beads: optimization and modelling using non-linear regression technique, *J. Water Process Eng.*, 2 (2014) 43–52.
- [79] S. Hosseini, M.A. Khan, M.R. Malekbala, W. Cheah, T.S. Choong, Carbon coated monolith, a mesoporous material for the removal of methyl orange from aqueous phase: adsorption and desorption studies, *Chem. Eng. J.*, 171 (2011) 1124–1131.
- [80] A. Asfaram, M. Ghaedi, S. Hajati, M. Rezaeinejad, A. Goudarzi, M.K. Purkait, Rapid removal of Auramine-O and Methylene blue by ZnS: Cu nanoparticles loaded on activated carbon: a response surface methodology approach, *J. Taiwan Inst. Chem. Eng.*, 53 (2015) 80–91.
- [81] J. Sharma, B.S. Kaith, A.K. Sharma, A. Goel, Gum xanthan-pssyllium-cl-poly (acrylic acid-co-itaconic acid) based adsorbent for effective removal of cationic and anionic dyes: adsorption isotherms, kinetics and thermodynamic studies, *Ecotoxicol. Environ. Saf.*, 149 (2018) 150–158.
- [82] M. Jafari, M.R. Rahimi, M. Ghaedi, K. Dashtian, ZnO nanoparticles loaded different mesh size of porous activated carbon prepared from *Pinus eldarica* and its effects on simultaneous removal of dyes: multivariate optimization, *Chem. Eng. Res. Des.*, 125 (2017) 408–421.
- [83] E.A. Dil, M. Ghaedi, A. Ghaedi, A. Asfaram, A. Goudarzi, S. Hajati, M. Soylak, S. Agarwal, V.K. Gupta, Modeling of quaternary dyes adsorption onto ZnO-NR-AC artificial neural network: analysis by derivative spectrophotometry, *J. Ind. Eng. Chem.*, 34 (2016) 186–197.
- [84] K. Dashtian, S. Porhemat, A.R. Rezvani, M. Ghaedi, M.M. Sabzehmeidani, Adsorption of semisoft pollutants onto Bi<sub>2</sub>S<sub>3</sub>/Ag<sub>2</sub>S-AC under the influence of ultrasonic waves as external field, *J. Ind. Eng. Chem.*, 60 (2018) 390–400.
- [85] M. Jamshidi, M. Ghaedi, K. Dashtian, S. Hajati, A. Bazrafshan, Sonochemical assisted hydrothermal synthesis of ZnO: Cr

- nanoparticles loaded activated carbon for simultaneous ultrasound-assisted adsorption of ternary toxic organic dye: derivative spectrophotometric, optimization, kinetic and isotherm study, *Ultrason. Sonochem.*, 32 (2016) 119–131.
- [86] S. Jana, J. Ray, B. Mondal, T. Tripathy, Efficient and selective removal of cationic organic dyes from their aqueous solutions by a nanocomposite hydrogel, katira gum-cl-poly (acrylic acid-co-N, N-dimethylacrylamide)@ bentonite, *Appl. Clay Sci.*, 173 (2019) 46–64.
- [87] T.N.V. de Souza, S.M.L. de Carvalho, M.G.A. Vieira, M.G.C. da Silva, D.D.S.B. Brasil, Adsorption of basic dyes onto activated carbon: experimental and theoretical investigation of chemical reactivity of basic dyes using DFT-based descriptors, *Appl. Surf. Sci.*, 448 (2018) 662–670.